ELSEVIER

Mechanics of Materials 33 (2001) 335-362

MECHANICS OF MATERIALS

www.elsevier.com/locate/mechmat

On the use of planar shear-lag methods for stress-transfer analysis of multilayered composites

J.A. Nairn[a,*], **D.A. Mendels**[b]

[a] *Material Science & Engineering, Room 304, 122 S. Central Campus Drive, University of Utah, Salt Lake City, UT 84112, USA*

[b] *Laboratoire de Technologie des Composites et Polymères (LTC), Ecole Polytechnique Fédérale de Lausanne (EPFL), CH-1015 Lausanne, Switzerland*

Received 13 September 2000; received in revised form 30 January 2001

Abstract

Shear-lag equations for analysis of stresses in a multilayered composite were derived using a series of approximations to exact two-dimensional elasticity methods. The shear-lag equations derived with the fewest assumptions was termed the *Optimal, Shear-Lag Analysis* for planar problems in composites. A solution method for these equations was outlined based on eigen-analysis of a matrix of shear-lag parameters. The optimal, shear-lag analysis differs from most prior shear-lag methods in the literature. By adding more assumptions, we could reduce the optimal analysis to two common, prior shear-lag methods. These prior methods were labeled as *Interlayer, Shear-Lag Analysis* and *Parametric, Interlayer, Shear-Lag Analysis*. Because theses two interlayer methods required more assumptions than the optimal method, they are less accurate than that method. Several examples illustrated the types of problems that can be accurately solved by shear-lag analysis and the differences in accuracy between the various shear lag methods. The results of this paper can be used to guide the derivation of future, improved shear-lag models or to evaluate the quality of prior shear-lag models.

1. Introduction

Shear-lag analysis as a tool for stress analysis in composite materials is usually traced to Cox (1952). In a brief section of that paper, Cox proposed a simple one-dimensional, equation for analyzing stress transfer between a fiber and a matrix. This initial work considered a single fiber in a matrix or an axisymmetric stress-analysis geometry. There have been many subsequent, axisymmetric, shear-lag analyses (*e.g.*, Gau, Mai, and Cotterell, 1988; Hsueh, 1988; Hsueh, 1995; Kim, Baillie, and Mai, 1991; Lacroix, Tilmans, Keunings, Desaeger, and Verpoest, 1992; Liu and Nairn, 1999; McCartney, 1992; Nairn and Wagner, 1996; Nayfeh, 1977; Piggott, 1987; Zhou, Kim, and Mai, 1992). A recent paper considered axisymmetric shear-lag analysis in detail and showed how Cox's original equation can be derived by a series of approximations to methods of axisymmetric elasticity (Nairn, 1997). This analysis gave more insight into the accuracy of axisymmetric shear-lag methods. When done correctly (McCartney, 1992; Liu and Nairn, 1999; Nairn and Wagner, 1996; Nairn, 1997; Nayfeh, 1977), which means the *shear-lag parameter* must be calculated correctly and *not* calculated the way originally suggested by Cox (1952), axisymmetric shear-lag analysis can lead to excellent results for finding axial stresses and displacement in fibers embedded in a matrix (Nairn, 1997) and for finding energy release rate for some crack-growth problems (Liu and Nairn, 1999). It is less accurate for finding interfacial shear stresses, although it is often misused for that purpose. It should not be expected to be accurate for much else.

Shear-lag analysis of composites has also found many uses in planar problems. One early example is the shear-lag analysis of unidirectional composites developed by Hedgepeth (1961; Hedgepeth and Van Dyke,

*Corresponding Author: Tel:+1-541-737-4265, Fax:+1-541-737-3385 (updated 2006).
E-mail address: John.Nairn@oregonstate.edu (J.A. Nairn) (updated 2006)

1967). Although this work imagined cylindrical fibers, it is mathematically a planar analysis of a multilayered structure with alternating fiber and matrix layers. Shear-lag models based on Hedgepeth's approach have often been used to study stress analysis problems in unidirectional composites (*e.g.*, Dharani, Jones, and Goree, 1983; Eringren and Kim, 1944; Goree and Gross, 1979b; Goree and Gross, 1979a; Hedgepeth, 1961; Hedgepeth and Van Dyke, 1967; Kulkarni, Rosen, and Zweben, 1973; Nairn, 1988a; Nairn, 1988b; Nairn, Liu, Chen, and Wedgewood, 1990; Phoenix and Beyerlein, 2000). Planar shear-lag methods have also been used to study laminates where the $x-y$ analysis plane becomes the edge of the laminate and the layers in the model become the plies in the laminate. Such models have frequently been used to analyze stresses around matrix cracks in 90° plies (*e.g.*, Caslini, Zanotti, and O'Brien, 1987; Dharani and Tang, 1990; Flaggs, 1985; Garrett and Bailey, 1977; Han, Hahn, and Croman, 1987a; Han, Hahn, and Croman, 1987b; Laws and Dvorak, 1988; Manders, Chou, Jones, and Rock, 1983; McCartney, 1992; McManus and Maddocks, 1996; Reifsnider, 1977; Tan and Nuismer, 1990). When the planar *shear-lag parameter* is calculated correctly (McCartney, 1992) (and most such analyses calculate it inaccurately), shear-lag analysis does an excellent job of predicting the effect of microcracks on the axial modulus of the laminate (McCartney, 1992; Nairn, 2000). It is not as accurate for making predictions of microcrack formation based on the energy release rate due to the formation of the next microcrack (Nairn, 2000; Nairn, Hu, and Bark, 1993; Nairn and Hu, 1994).

This paper considers shear-lag analysis for planar problems using methods similar to those in the previous paper (Nairn, 1997) that considered the use of shear-lag analysis for axisymmetric problems. We began with the fundamental shear-lag assumption, which is an assumption common to all planar shear-lag analyses, and derived the classes of stress states that *exactly* satisfy that assumption. These stress states do not solve any interesting composite stress analysis problems, but they provided guidance to the development of approximate shear-lag methods. By relaxing the form of the shear stress and introducing a few other assumptions, we derived a new shear-lag analysis for multilayered structures. We termed this analysis method an *optimal* shear-lag analysis because it is based on the fewest assumptions. The optimal, shear-lag analysis differs from most previous shear-lag analyses, such as those based on Hedgepeth (1961). By introducing more assumptions, however, it was possible to reduce the optimal, shear-lag analysis to a Hedgepeth-type analysis. Adding yet another assumption reproduced another class of shear-lag analyses common in the literature. The process of starting from elasticity theory and deriving various shear-lag models by successive approximations can be used to categorize most planar shear-lag models in the literature and rank them by expected accuracy. The optimal, shear-lag and the Hedgepeth-like, shear-lag analyses were applied to several sample calculations.

The intent of this paper was not to advocate shear-lag analysis as a preferred method for stress analysis of composites. There are many limitations to the types of problems that can be analyzed and to the type of results that can be generated by shear-lag methods. But, the shear-lag equations are usually amenable to simple solutions that makes it possible to get results. When shear-lag analysis is done correctly, those easily-derived results can also be accurate results. This paper can be used as a guide to deriving optimal or sub-optimal, shear-lag analyses and to assessing both their capabilities and their limitations.

2. Theory

Shear-lag analyses in the composites literature always contain several approximations although a complete specification of assumptions is usually not given. A feature common to all shear-lag analysis is that one assumption always involves a simplification of in-plane shear stress, τ_{xy}, to decouple the x and y directions. This decoupling permits 2D-planar elasticity problems to be simplified to a 1D analysis. The standard shear-stress simplification is to assume that

$$\tau_{xy} \propto \frac{\partial v}{\partial x} \tag{1}$$

where v is displacement in the y direction. By exact linear elasticity, the shear stress is

$$\tau_{xy} = G_{xy}\gamma_{xy} = G_{xy}\left(\frac{\partial v}{\partial x} + \frac{\partial u}{\partial y}\right) \tag{2}$$

where G_{xy} is in-plane shear modulus, γ_{xy} is in-plane shear strain, and u is displacement in the x direction. Thus, although it is not usually stated in the following form, the fundamental assumption common to all

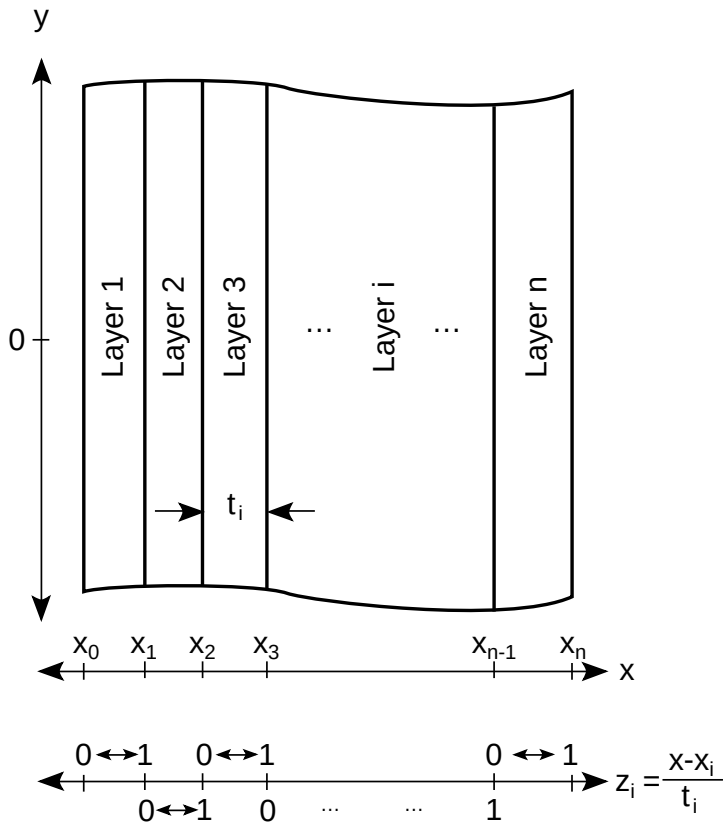

Fig. 1. The geometry of an n-layered composite. Layer i extends from x_{i-1} to x_i and has thickness t_i, tensile moduli $E_x^{(i)}$ and $E_y^{(i)}$, in-plane shear modulus $G_{xy}^{(i)}$, in-plane Poisson's ratio $\nu_{xy}^{(i)}$, and thermal expansion coefficients $\alpha_x^{(i)}$ and $\alpha_y^{(i)}$. The z_i coordinate is a dimensionless coordinate in layer i that varies from 0 and 1 in that layer.

planar, shear-lag analyses is that

$$\frac{\partial u}{\partial y} = 0, \quad \text{or at least that} \quad \left|\frac{\partial u}{\partial y}\right| << \left|\frac{\partial v}{\partial x}\right| \tag{3}$$

In this section, we consider application of this fundamental shear-lag approximation to 2D plane-stress or plain-strain, stress analysis problems. The composite geometry analyzed is the n-layered composite shown in Fig. 1. The layers are assumed to be linear thermoelastic with orthotropic mechanical properties and thermal expansion coefficients that are independent of temperature. Layer i extends from x_{i-1} to x_i and therefore has thickness $t_i = x_i - x_{i-1}$. The x- and y-direction tensile moduli, in-plane shear modulus, and in-plane Poisson's ratio of layer i are $E_x^{(i)}$, $E_y^{(i)}$, $G_{xy}^{(i)}$, and $\nu_{xy}^{(i)}$, respectively. The x- and y-direction thermal expansion coefficients are $\alpha_x^{(i)}$ and $\alpha_y^{(i)}$. Attention is focused on n-layered composites subjected to axial loading in the y direction, possibly in-plane shear loading, and thermal loading of $\Delta T = T - T_0$ where T is the current temperature and T_0 is the reference stress-free temperature. In linear, thermoelastic composites with temperature independent properties, T_0 might be the processing temperature. Temperature-dependent effects and viscoelastic relaxation of residual stresses can be handled by setting T_0 to an *effective* stress-free temperature such that ΔT in a linear-thermoelastic analysis recovers the true level of residual stresses.

Exact Shear-Lag Results

It is instructive to consider all possible stress states that are exact solutions to elasticity problems and simultaneously satisfy the fundamental shear-lag approximation. Any stress state that does not fall within

this class of stress states can only be analyzed approximately by shear-lag analysis; the more a composite stress state differs from the possible exact stress states, the less accurate will be the shear-lag analysis for that stress state.

Let $\phi(x,y)$ be an Airy stress function (Timoshenko, 1970) for planar analysis of layer i such that the in-plane stresses, which automatically satisfy equilibrium, are given by:

$$\sigma_x = \frac{\partial^2\phi}{\partial y^2}, \qquad \sigma_y = \frac{\partial^2\phi}{\partial x^2}, \qquad \text{and} \qquad \tau_{xy} = -\frac{\partial^2\phi}{\partial x\partial y} \tag{4}$$

The in-plane normal and shear strains, for possibly anisotropic material properties, are given by

$$\varepsilon_x = \frac{\partial u}{\partial x} = \frac{\sigma_x}{E_x^{(i)}} - \frac{\nu_{xy}^{(i)}\sigma_y}{E_x^{(i)}} + \alpha_x^{(i)}\Delta T \tag{5}$$

$$\varepsilon_y = \frac{\partial v}{\partial y} = \frac{\sigma_y}{E_y^{(i)}} - \frac{\nu_{xy}^{(i)}\sigma_x}{E_x^{(i)}} + \alpha_y^{(i)}\Delta T \tag{6}$$

$$\gamma_{xy} = \frac{\partial v}{\partial x} + \frac{\partial u}{\partial y} = \frac{\tau_{xy}}{G_{xy}^{(i)}} \tag{7}$$

Substituting these strains in the 2D compatibility condition for in-plane strains, $\phi(x,y)$ must satisfy the fourth order differential equation (Lekhnitski, 1981):

$$\frac{1}{E_y^{(i)}}\frac{\partial^4\phi}{\partial x^4} + \left(\frac{1}{G_{xy}^{(i)}} - \frac{2\nu_{xy}^{(i)}}{E_x^{(i)}}\right)\frac{\partial^4\phi}{\partial x^2\partial y^2} + \frac{1}{E_x^{(i)}}\frac{\partial^4\phi}{\partial y^4} = 0 \tag{8}$$

The fundamental shear-lag assumption implies that u, and therefore also ε_x, are functions only of x. Thus differentiating eq. (5) with respect to y leads to

$$\frac{\partial}{\partial y}\left[\frac{1}{E_x^{(i)}}\frac{\partial^2\phi}{\partial y^2} - \frac{\nu_{xy}^{(i)}}{E_x^{(i)}}\frac{\partial^2\phi}{\partial x^2}\right] = 0 \tag{9}$$

Additionally, differentiating eq. (6) with respect to x and equating to eq. (7) differentiated with respect to y, while using the fundamental shear-lag assumption, leads to

$$\frac{\partial}{\partial x}\left[\frac{1}{E_y^{(i)}}\frac{\partial^2\phi}{\partial x^2} + \left(\frac{1}{G_{xy}^{(i)}} - \frac{\nu_{xy}^{(i)}}{E_x^{(i)}}\right)\frac{\partial^2\phi}{\partial y^2}\right] = 0 \tag{10}$$

Any function $\phi(x,y)$ which satisfies both eqs (9) and (10) will give a stress state that satisfies the fundamental shear-lag assumption. Because it is easy to show that all such $\phi(x,y)$ also satisfy eq. (8), the possible solutions to eqs (9) and (10) define all exact shear-lag analysis stress states. Equation (9) implies that the square bracketed term can be written as $f(x)$ which is an arbitrary function of x only. Similarly, eq. (10) implies that the square-bracketed term can be written as an arbitrary function of y only, $g(y)$. Equating the square-bracketed terms to these equations and solving for the derivatives of the $\phi(x,y)$ function gives

$$\sigma_x = \frac{\partial^2\phi}{\partial y^2} = \frac{\nu_{xy}^{(i)}}{E_x^{(i)}}g(y) + \frac{1}{E_y^{(i)}}f(x) \tag{11}$$

$$\sigma_y = \frac{\partial^2\phi}{\partial x^2} = \frac{1}{E_x^{(i)}}g(y) - \left(\frac{1}{G_{xy}^{(i)}} - \frac{\nu_{xy}^{(i)}}{E_x^{(i)}}\right)f(x) \tag{12}$$

Differentiating eq. (11) twice with respect to x and equating to eq. (12) differentiated twice with respect to y gives

$$f''(x) = \frac{E_y^{(i)}}{E_x^{(i)}}g''(y) \tag{13}$$

This result implies that $f''(x)$ and $g''(y)$ must be constants independent of x and y, which further implies that $f(x)$ is quadratic in x and $g(y)$ is quadratic in y.

Finally, all possible stress states that exactly satisfy the fundamental shear-lag assumptions can be written in the form:

$$\sigma_x = b_0 + b_1 x + a_2 x^2 + (a_0 + a_1 y + a_2 y^2)\nu_{xy}^{(i)} \tag{14}$$

$$\sigma_y = a_0 + a_1 y + a_2 y^2 - \left(b_0 + b_1 x + a_2 x^2\right)\left(\frac{E_y^{(i)}}{G_{xy}^{(i)}} - \nu_{yx}^{(i)}\right) \tag{15}$$

$$\tau_{xy} = b_2 - b_1 y - (a_1 + 2a_2 y)\, x \tag{16}$$

where a_i and b_i are constants. The shear stress was found from the two tensile stresses by integrating the 2D equations of stress equilibrium. Shear-lag analyses of multilayered composites are often used for problems involving stress transfer between the layers through shear at the interfaces. In the exact shear-lag stress states, interfacial shear stresses (τ_{xy} at constant x_i) are linear in y. Linear interfacial shear stresses leads to quadratic variations in the average axial stress ($\langle\sigma_y\rangle$) in any layer.

Optimal, Approximate Shear-Lag Analysis

If shear-lag analysis was limited to stress states having the form of the exact stress states derived in the previous section, it would not solve any interesting composite stress analysis problems. To solve more complex problems by shear-lag analysis requires an *approximate shear-lag* method. One approach to deriving an approximate method is to relax the constraints of the exact stress states (McCartney, 1992). We allowed τ_{xy} to have a more general form; we assumed $\tau_{xy}^{(i)}$ in layer i to have the form:

$$\tau_{xy}^{(i)} = f_0^{(i)}(x)g_0^{(i)}(y) + f_1^{(i)}(x)g_1^{(i)}(y) \tag{17}$$

In the exact stress states, $g_0^{(i)}(y)$ and $g_1^{(i)}(y)$ are linear in y, $f_0^{(i)}(x)$ is a constant, and $f_1^{(i)}(x)$ is linear in x. In this approximate analysis we allow $g_i^{(i)}(y)$ and $f_i^{(i)}(x)$ to have any variations with y and x. The goal of this section is to derive shear-lag equations that can be used to determine these new functions or to determine the stresses in the layers. We define an optimal, approximate shear-lag analysis as the one that derives the final equations with minimal additional assumptions to supplement the fundamental shear-lag assumption.

First, we defined z_i as a dimensionless coordinate in the x direction in each layer as

$$z_i = \frac{x - x_{i-1}}{t_i} \tag{18}$$

z_i varies from 0 to 1 through the thickness of each layer (see Fig. 1). Second, we defined layer *shape* function $L_i(z_i)$ and $R_i(z_i)$ that are functions only of z_i having the properties

$$L_i(0) = 1, \qquad L_i(1) = 0, \qquad R_i(0) = 0, \qquad \text{and} \qquad R_i(1) = 1 \tag{19}$$

$L_i(z_i)$ is the *left-side* shape function that is 1 on the left edge of the layer and 0 on the right edge of the layer; similarly, $R_i(z_i)$ is the *right-side* shape function. Third, we defined $\tau(x_i)$ as the interfacial shear stress at the interface between layer i and $i+1$ located at x_i. In terms of dimensionless coordinates, shape functions, and interfacial shear stresses, the layer shear stress in eq. (17) can be rewritten as

$$\tau_{xy}^{(i)} = \tau(x_{i-1})L_i + \tau(x_i)R_i \tag{20}$$

Some previous shear-lag analyses treat $\tau_{xy}^{(i)}$ as linear in x in each layer (McCartney, 1992). This new analysis can derive such linear results by setting $L_i(z_i) = 1 - z_i$ and $R_i(z_i) = z_i$. But, it is also possible to derive shear-lag equations without requiring the shape functions to be linear. The examples in this paper show how the use of non-linear shape functions can improve the accuracy of shear-lag methods.

From eq. (7), the fundamental shear-lag assumption ($\partial u/\partial y = 0$), and eq. (20)

$$\frac{\partial v}{\partial z_i} = \frac{t_i}{G_{xy}^{(i)}}\left(\tau(x_{i-1})L_i + \tau(x_i)R_i\right) \tag{21}$$

Using a transform method developed by McCartney (McCartney, 1992), we multiply both sides of eq. (21) by $(A - z_i)$ and integrate by parts over the layer thickness to get

$$\left\langle v^{(i)} \right\rangle + v(x_i)(A-1) - v(x_{i-1})A = \frac{t_i \tau(x_{i-1})}{G_{xy}^{(i)}} \left(A \langle L_i \rangle - \langle z_i L_i \rangle \right) + \frac{t_i \tau(x_i)}{G_{xy}^{(i)}} \left(A \langle R_i \rangle - \langle z_i R_i \rangle \right) \tag{22}$$

where $\langle \cdot \rangle$ indicates averaging over the thickness of the layer such as

$$\left\langle v^{(i)} \right\rangle = \frac{1}{t_i} \int_{x_{i-1}}^{x_i} v(x,y)\, dx = \int_0^1 v(z_i, y)\, dz_i \tag{23}$$

The terms $v(x_i)$ and $v(x_{i-1})$ are the axial displacements on the two edges of layer i. By continuity of axial displacements, these edge displacements must equal the corresponding edge displacements in layers $i-1$ and $i+1$, respectively. This shear-lag analysis thus satisfies continuity in both shear stresses and axial displacements. The terms $\left\langle v^{(i)} \right\rangle$, $v(x_i)$, and $v(x_{i-1})$ are functions of y only. The terms $\langle L_i \rangle$, $\langle z_i L_i \rangle$, $\langle R_i \rangle$, and $\langle z_i R_i \rangle$ are all constants depending on the choice of shape functions. Setting $A = 1$ for layer $i+1$ and $A = 0$ for layer i, respectively, gives two relations

$$\left\langle v^{(i+1)} \right\rangle = v(x_i) + \frac{t_{i+1}\tau(x_i)}{G_{xy}^{(i+1)}} \langle (1 - z_{i+1}) L_{i+1} \rangle + \frac{t_{i+1}\tau(x_{i+1})}{G_{xy}^{(i+1)}} \langle (1 - z_{i+1}) R_{i+1} \rangle \tag{24}$$

$$\left\langle v^{(i)} \right\rangle = v(x_i) - \frac{t_i \tau(x_{i-1})}{G_{xy}^{(i)}} \langle z_i L_i \rangle - \frac{t_i \tau(x_i)}{G_{xy}^{(i)}} \langle z_i R_i \rangle \tag{25}$$

Subtracting eq. (25) from eq. (24) gives

$$\begin{aligned} \left\langle v^{(i+1)} \right\rangle - \left\langle v^{(i)} \right\rangle = {} & \frac{t_{i+1} \langle (1 - z_{i+1}) R_{i+1} \rangle}{G_{xy}^{(i+1)}} \tau(x_{i+1}) + \frac{t_i \langle z_i L_i \rangle}{G_{xy}^{(i)}} \tau(x_{i-1}) \\ & + \left(\frac{t_{i+1} \langle (1 - z_{i+1}) L_{i+1} \rangle}{G_{xy}^{(i+1)}} + \frac{t_i \langle z_i R_i \rangle}{G_{xy}^{(i)}} \right) \tau(x_i) \end{aligned} \tag{26}$$

A second relation between displacement and shear stress can be derived by using stress equilibrium and Hooke's law. By stress equilibrium in layer i

$$\frac{\partial \sigma_y^{(i)}}{\partial y} + \frac{\partial \tau_{xy}^{(i)}}{\partial x} = 0 \tag{27}$$

Integrating over the thickness of the layer, it is easy to show that

$$\frac{d\left(t_i \left\langle \sigma_y^{(i)} \right\rangle \right)}{dy} = \tau(x_{i-1}) - \tau(x_i) \tag{28}$$

Next, differentiate Hooke's law in eq. (6) with respect to y and average over the layer thickness to get

$$\frac{d^2 \left\langle v^{(i)} \right\rangle}{dy^2} = \frac{1}{E_y^{(i)} t_i} \frac{d\left(t_i \left\langle \sigma_y^{(i)} \right\rangle \right)}{dy} - \frac{\nu_{xy}^{(i)}}{E_x^{(i)}} \frac{d\left\langle \sigma_x^{(i)} \right\rangle}{dy} \tag{29}$$

To proceed we need to introduce a second shear-lag assumption. We assume that

$$\left| \frac{\nu_{xy}^{(i)}}{E_x^{(i)}} \frac{d\left\langle \sigma_x^{(i)} \right\rangle}{dy} \right| << \left| \frac{d\left\langle \sigma_y^{(i)} \right\rangle}{dy} \right| \tag{30}$$

Combining this assumption with eqs (28) and (29) and eliminating $\left\langle \sigma_y^{(i)} \right\rangle$ gives

$$\frac{d^2 \left\langle v^{(i)} \right\rangle}{dy^2} = \frac{\tau(x_{i-1}) - \tau(x_i)}{E_y^{(i)} t_i} \tag{31}$$

The assumption in eq. (30) is made in virtually all shear-lag analyses, although it is not always explicitly stated. It is typically introduced by making use of a 1D axial Hooke's law of

$$\varepsilon_y = \frac{\partial v}{\partial y} = \frac{\langle \sigma_y \rangle}{E_y^{(i)}} + \alpha_y^{(i)} \Delta T \tag{32}$$

instead of the full 2D relation in eq. (6). The assumption in eq. (30) is less severe than the use of a 1D Hooke's law. Here, we do not require $\langle \sigma_x \rangle$ to be much less than $\langle \sigma_y \rangle$, we only require that $\langle \sigma_x \rangle$ varies much slower in the y direction than does $\langle \sigma_y \rangle$. This assumptions is probably a good assumption for problems of stress transfer during loading in the y direction, which is a problem commonly analyzed by shear-lag methods.

Finally, differentiating eq. (26) twice with respect to y and making use of eq. (31) leads to

$$\begin{aligned} -\frac{\tau(x_{i+1})}{E_y^{(i+1)} t_{i+1}} + \left(\frac{1}{E_y^{(i+1)} t_{i+1}} + \frac{1}{E_y^{(i)} t_i} \right) \tau(x_i) - \frac{\tau(x_{i-1})}{E_y^{(i)} t_i} = \frac{t_{i+1} \langle (1 - z_{i+1}) R_{i+1} \rangle}{G_{xy}^{(i+1)}} \tau''(x_{i+1}) \\ + \frac{t_i \langle z_i L_i \rangle}{G_{xy}^{(i)}} \tau''(x_{i-1}) + \left(\frac{t_{i+1} \langle (1 - z_{i+1}) L_{i+1} \rangle}{G_{xy}^{(i+1)}} + \frac{t_i \langle z_i R_i \rangle}{G_{xy}^{(i)}} \right) \tau''(x_i) \end{aligned} \tag{33}$$

Equation (33) for $i = 1$ to $n-1$ defines a system of $n-1$ second order differential equations which can be solved to find the $n-1$ interfacial shear stresses in the n-layered composite. Defining $\boldsymbol{\tau} = (\tau(x_1), \tau(x_2), \ldots, \tau(x_{n-1}))$ as a vector of the interfacial shear stresses, the system of equations can be written as

$$[A] \frac{d^2 \boldsymbol{\tau}}{dy^2} - [B] \boldsymbol{\tau} = -\boldsymbol{\tau}_0 \tag{34}$$

where $[A]$ and $[B]$ are each tridiagonal matrices with elements

$$\begin{array}{lll} A_{i,i-1} = \dfrac{t_i \langle z_i L_i \rangle}{G_{xy}^{(i)}} & A_{i,i} = \dfrac{t_{i+1} \langle (1 - z_{i+1}) L_{i+1} \rangle}{G_{xy}^{(i+1)}} + \dfrac{t_i \langle z_i R_i \rangle}{G_{xy}^{(i)}} & A_{i,i+1} = \dfrac{t_{i+1} \langle (1 - z_{i+1}) R_{i+1} \rangle}{G_{xy}^{(i+1)}} \\ B_{i,i-1} = -\dfrac{1}{E_y^{(i)} t_i} & B_{i,i} = \dfrac{1}{E_y^{(i+1)} t_{i+1}} + \dfrac{1}{E_y^{(i)} t_i} & B_{i,i+1} = -\dfrac{1}{E_y^{(i+1)} t_{i+1}} \end{array} \tag{35}$$

The vector $\boldsymbol{\tau}_0$ allows the analysis to account for non-zero shear-stress boundary conditions on the left edge of layer 1 or on the right edge of layer n. This type of analysis can handle any variation in shear-stress boundary conditions; here we only consider constant shear stress boundary conditions which have $\tau''(x_0) = \tau''(x_n) = 0$. For such boundary conditions:

$$\boldsymbol{\tau}_0 = \left(\frac{\tau_0}{E_y^{(1)} t_1}, 0, \ldots, \frac{\tau_n}{E_y^{(n)} t_n} \right) \tag{36}$$

where τ_0 and τ_n are the constant shear stress boundary conditions on the left and right edges, respectively.

For solution purposes, it is convenient to rewrite eq. (34) as

$$\frac{d^2 \boldsymbol{\tau}}{dy^2} - [M_\tau] \boldsymbol{\tau} = -[M_\tau] \boldsymbol{\tau}_\infty \tag{37}$$

where $[M_\tau] = [A]^{-1}[B]$ and $\boldsymbol{\tau}_\infty = [B]^{-1} \boldsymbol{\tau}_0$. As shown in the appendix, the i^{th} element of $\boldsymbol{\tau}_\infty$ is

$$(\boldsymbol{\tau}_\infty)_i = \tau_0 + \sum_{j=1}^{i} \frac{t_j E_y^{(j)}}{t E_y^0} (\tau_n - \tau_0) \tag{38}$$

where $t = \sum_{i=1}^{n} t_i$ is total thickness of the composite and

$$E_y^0 = \frac{1}{t} \sum_{i=1}^{n} t_i E_y^{(i)} \tag{39}$$

is the rule-of-mixtures effective composite modulus of an undamaged structure in the y direction. Physically $\boldsymbol{\tau}_\infty$ gives the far-field or steady state interfacial shear stresses as an interpolation between τ_0 and τ_n weighted according to the stiffnesses of the intervening layers. These are the interfacial shear stresses far away from any end or from any discontinuities or breaks in any layers.

Once eq. (34) is solved for all interfacial shear stresses, the average axial stress in each layer can be determined by integration of eq. (28). Alternatively, it is convenient to transform eq. (34) into an equation for direct determination of the average axial layer stresses. By eq. (28) and an iterative analysis, the interfacial shear stresses can be written in terms of the average axial stresses by

$$\tau(x_i) = \tau_0 - \sum_{j=1}^{i} \frac{d\left(t_j \left\langle \sigma_y^{(j)} \right\rangle\right)}{dy} \tag{40}$$

Let $\mathbf{p} = (t_1 \left\langle \sigma_y^{(1)} \right\rangle, t_2 \left\langle \sigma_y^{(2)} \right\rangle, \ldots, t_{n-1} \left\langle \sigma_y^{(n-1)} \right\rangle)$ be a vector of forces per unit plate depth on the layers. In matrix form, $\boldsymbol{\tau}$ becomes

$$\boldsymbol{\tau} = \tau_0(1, 1, \ldots, 1) - [I_L]\frac{d\mathbf{p}}{dy} \tag{41}$$

where $[I_L]$ is an $(n-1) \times (n-1)$ matrix with all diagonal and lower half-diagonal elements equal to one while all upper half-diagonal elements are zero (*i.e.*, $(I_L)_{i,j} = 1$ if $i \geq j$, otherwise $(I_L)_{i,j} = 0$). Substitution into eq. (34) gives

$$\frac{d^3\mathbf{p}}{dy^3} - [M_\sigma]\frac{d\mathbf{p}}{dy} = -[M_\sigma]\frac{d\mathbf{p}_\infty}{dy} \tag{42}$$

where

$$[M_\sigma] = [I_L]^{-1}[M_\tau][I_L] \tag{43}$$

and the i^{th} element of $d\mathbf{p}_\infty/dy$ is

$$\left(\frac{d\mathbf{p}_\infty}{dy}\right)_i = [I_L]^{-1}\big(\tau_0(1, 1, \ldots, 1) - \boldsymbol{\tau}_\infty\big) = \frac{t_i E_y^{(i)}}{t E_y^0}\big(\tau_0 - \tau_n\big) \tag{44}$$

The final form of $d\mathbf{p}_\infty/dy$ was derived by noting that $[I_L]^{-1}$ has all diagonal elements equal to one, all elements immediately below the diagonal equal to -1, and all other elements zero (*i.e.*, $(I_L)^{-1}_{i,i} = 1$, $(I_L)^{-1}_{i,i-1} = -1$, otherwise $(I_L)^{-1}_{i,j} = 0$). Integrating eq. (42) once gives

$$\frac{d^2\mathbf{p}}{dy^2} - [M_\sigma]\mathbf{p} = -[M_\sigma]\mathbf{p}_\infty \tag{45}$$

The integration constant, which here has been incorporated into $\mathbf{p}_\infty$, must be the far-field or steady state tensile stresses in each layer when there are no shear stress boundary conditions; in other words, the tensile forces in the layers under constant axial stress far away from any end or from any discontinuities or breaks in any layers. Combining this constant term with the integrated shear stress terms in eq. (44) gives the i^{th} element of $\mathbf{p}_\infty$ as

$$(\mathbf{p}_\infty)_i = E_y^{(i)} t_i \left[\frac{\big(\tau_0 - \tau_n\big)y + t\sigma_0(0)}{t E_y^0} + (\alpha_y^0 - \alpha_y^{(i)})\Delta T\right] \tag{46}$$

where $\sigma_0(0)$ is the total applied stress in the y direction when $y = 0$, and α_y^0 is the rule-of-mixtures effective y-direction thermal expansion coefficient of an undamaged structure given by

$$\alpha_y^0 = \sum_{i=1}^{n} \frac{\alpha_y^{(i)} t_i E_y^{(i)}}{t E_y^0} \tag{47}$$

Note that $\sigma_0(y) = \big(\tau_0 - \tau_n\big)y + \sigma_0(0)$ is the total applied axial stress in the y direction for problems with constant, non-zero shear stresses applied to the sides of the specimen. When there are no shear-stress boundary conditions, $\sigma_0(y)$ is constant and equal to the total applied axial stress.

Solution Method and Properties

The solution to the system of coupled second-order differential equations in eq. (45) that has no first-derivative terms can be written down using the eigenvalues and eigenvector of the matrix $[M_\sigma]$. Making use of the obvious particular solution of $\mathbf{p}_{part} = \mathbf{p}_\infty$, the average stress in each layer is:

$$\left\langle \sigma_y^{(i)} \right\rangle = E_y^{(i)} \left[\frac{\big(\tau_0 - \tau_n\big)y + t\sigma_0(0)}{tE_y^0} + (\alpha_y^0 - \alpha_y^{(i)})\Delta T \right] + \sum_{j=1}^{n-1} \left(a_j e^{\lambda_j y} + b_j e^{-\lambda_j y} \right) \frac{\psi_{j,i}}{t_i} \tag{48}$$

Here λ_j^2 for $j = 1$ to $n-1$ are the eigenvalues of $[M_\sigma]$ and $\psi_{j,i}$ is the i^{th} element of the corresponding eigenvector. The $2(n-1)$ unknown constants a_j and b_j for $j = 1$ to $n-1$ must be determined by boundary conditions. Making use of eq. (40), the interfacial shear stresses are:

$$\tau(x_i) = \tau_0 + \sum_{k=1}^{i} \frac{t_k E_y^{(k)}}{tE_y^0} \big(\tau_n - \tau_0\big) - \sum_{k=1}^{i} \sum_{j=1}^{n-1} \left(a_j e^{\lambda_j y} - b_j e^{-\lambda_j y} \right) \lambda_j \psi_{j,k} \tag{49}$$

Alternatively, the solution for interfacial shear stresses can be found by an eigen-analysis of eq. (37) as:

$$\tau(x_i) = \tau_0 + \sum_{j=1}^{i} \frac{t_j E_y^{(j)}}{tE_y^0} (\tau_n - \tau_0) + \sum_{j=1}^{n-1} \left(a_j e^{\lambda_j y} - b_j e^{-\lambda_j y} \right) \omega_{j,i} \tag{50}$$

Here λ_j^2 for $j = 1$ to $n-1$ are the eigenvalues of $[M_\tau]$ matrix, which are identical to the eigenvalues of the $[M_\sigma]$ matrix because the transformation in eq. (43) leaves eigenvalues unchanged. $\omega_{j,i}$ is the i^{th} element of the eigenvector of $[M_\tau]$ associated with λ_j^2 and a_j and b_j for $j = 1$ to $n-1$ are constants determined by boundary conditions. Because these two shear stress results must be identical, the eigenvectors of $[M_\sigma]$ and $[M_\tau]$ must be related by:

$$\omega_{j,i} = -\sum_{k=1}^{i} \lambda_j \psi_{j,k} \qquad \text{or} \qquad \psi_{j,i} = \frac{\omega_{j,i-1} - \omega_{j,i}}{\lambda_j} \tag{51}$$

In terms of the eigenvectors of $[M_\tau]$, the average stress in each layer is:

$$\left\langle \sigma_y^{(i)} \right\rangle = E_y^{(i)} \left[\frac{\big(\tau_0 - \tau_n\big)y + t\sigma_0(0)}{tE_y^0} + (\alpha_y^0 - \alpha_y^{(i)})\Delta T \right] + \sum_{j=1}^{n-1} \left(a_j e^{\lambda_j y} + b_j e^{-\lambda_j y} \right) \frac{\omega_{j,i-1} - \omega_{j,i}}{t_i \lambda_j} \tag{52}$$

This *optimal* shear-lag solution satisfies axial equilibrium exactly, satisfies the simplified shear Hooke's law exactly (eq. (7) ignoring the $\partial u/\partial y$ term), and satisfies the simplified axial Hooke's law (eq. (6) ignoring the σ_x term) in an averaged sense. At the interfaces between layers, both the interfacial shear stress and the axial displacement are continuous.

The matrices $[M_\tau]$ and $[M_\sigma]$ are fully populated and not symmetric. Although an eigenanalysis of such general matrices can be difficult (Press, Flannery, Teukolsky, and Vetterling, 1988), there are some simplifications that make this analysis straight forward. First, on physical grounds, $[M_\tau]$ must be positive definite (*i.e.*, $\lambda_j^2 > 0$). The eigenvalue problem for the unsymmetric $[M_\tau]$ can thus be converted to an easier problem by forming the new matrix $[M_\tau][M_\tau]^T$ which is symmetric and has eigenvalues λ_j^4; the eigenvalues of this symmetric matrix can be found with standard numerical methods (Press, Flannery, Teukolsky, and Vetterling, 1988). Once λ_j^2 are known, the eigenvectors can be found by an iterative method. Because $[M_\tau]$ comes from two tridiagonal matrices, the equations for the eigenvectors can be rewritten as

$$[B]\vec{\omega_j} = \lambda_j^2 [A]\vec{\omega_j} \tag{53}$$

For each eigenvalue, one can set $\omega_{j,1} = 1$, substitute into eq. (53), and find all remaining elements using

$$\omega_{j,2} = \frac{B_{11} - \lambda_j^2 A_{11}}{\lambda_j^2 A_{12} - B_{12}} \tag{54}$$

$$\omega_{j,i+1} = \frac{(B_{i,i-1} - \lambda_j^2 A_{i,i-1})\omega_{j,i-1} + (B_{i,i} - \lambda_j^2 A_{i,i})\omega_{j,i}}{\lambda_j^2 A_{i,i+1} - B_{i,i+1}} \qquad \text{for } i = 2 \text{ to } n-1 \tag{55}$$

If necessary, the eigenvalues and eigenvectors respond well to refinement by inverse iteration (Press, Flannery, Teukolsky, and Vetterling, 1988); such refinement was not needed for the calculations in this paper.

This one-dimensional, optimal, shear-lag analysis determines only the average y-direction tensile stresses, the in-plane shear stresses, and the axial displacements. There have been various attempts to develop two-dimensional shear-lag methods. For example, because τ_{xy} is known every place, one could, in principle, substitute that stress into the transverse equilibrium equation.

$$\frac{\partial \sigma_x^{(i)}}{\partial x} + \frac{\partial \tau_{xy}^{(i)}}{\partial y} = 0 \tag{56}$$

differentiate and then integrate to find the transverse stress and similarly find the transverse displacements. In an analysis of axisymmetric shear-lag methods, it was found that shear-lag analysis is most accurate for finding axial stresses and displacements. It is less accurate for finding shear stresses because they are determined by differentiation of the approximate shear stresses (*e.g.* eq. (28)); any inaccuracies in the tensile stresses will get amplified by the differentiation step. Finding transverse stress and displacement using eq. (56) requires another differentiation step. It is unlikely that shear-lag analysis for average tensile stress is sufficiently accurate that a second derivative can be used to find transverse stresses and displacements. Furthermore, the transverse results will not satisfy any Hooke's laws exactly, approximately, or in an averaged sense. We suggest that shear-lag analysis of multilayered systems is only suitable for finding axial stresses and axial displacements. It may be sufficiently robust for determining interfacial shear stress also, but probably with less accuracy than the axial terms. For problems that require analysis of transverse stresses, it is probably necessary to abandon shear-lag methods and adopt approximate two-dimensional methods such as those developed by McCartney (1996; McCartney and Pierce, 1997) for multilayered structures.

The eigenvalues and eigenvectors in the above solutions depend on the particular choice for the shape functions that describe the variation of shear stresses in the x direction in each layer. Note that most previous shear-lag methods begin by introducing some assumption about the form of the shear stresses. Such analyses need to restart from the beginning to change that assumption. The analysis here leaves the form of the shear stresses undetermined. The final equations depend only on four dimensionless averages of the shape functions in each layer: $\langle z_i L_i \rangle$, $\langle (1-z_i) L_i \rangle$, $\langle z_i R_i \rangle$, and $\langle (1-z_i) R_i \rangle$. An optimal, shear-lag analysis for any desired assumptions about shear stresses can be generated simply by evaluating these constants and using them in the $[A]$ matrix. A common approach in previous shear-lag analyses, is to assume the x variation in all layers is linear which implies $L_i = 1 - z_i$ and $R_i = z_i$ and results in

$$\langle z_i L_i \rangle = \frac{1}{6}, \qquad \langle (1-z_i) L_i \rangle = \frac{1}{3}, \qquad \langle z_i R_i \rangle = \frac{1}{3}, \qquad \text{and} \qquad \langle (1-z_i) R_i \rangle = \frac{1}{6} \tag{57}$$

Interlayer, Shear-Lag Analysis

There is a large literature on planar shear-lag analyses of unidirectional composites based on the shear-lag analysis of Hedgepeth (1961). Hedgepeth analyzed specimens with an infinite number of fibers, but his methods can be applied to geometries with a finite number of fibers (Nairn, 1988a). The final equations for the axial stresses in a Hedgepeth-type, shear-lag analysis differs from the optimal, shear-lag result in eq. (45). In this section, we show how the Hedgepeth-type analysis can be derived from elasticity theory in a manner similar to that used above to derive the optimal, shear-lag analysis. The Hedgepeth-type derivation requires additional assumptions and thus must be less accurate than the optimal, shear-lag analysis.

The layers for analysis of a unidirectional composite are shown in Fig. 2. This geometry is identical to Fig. 1, except that n is always odd, all odd-i layers are matrix layers or *interlayers*, and all even-i layers are fiber layers. One new assumption of a Hedgepeth-type analysis is that all fiber layers are much stiffer than any matrix layers. When the fibers are sufficiently stiff, we can ignore shear deformations in the fiber and thus

$$\frac{\partial v}{\partial x} = 0 \qquad \text{for fiber layers } (i \text{ even}) \tag{58}$$

Integration leads to

$$\left\langle v^{(i)} \right\rangle = v(x_{i-1}) = v(x_i) \qquad \text{for } i \text{ even} \tag{59}$$

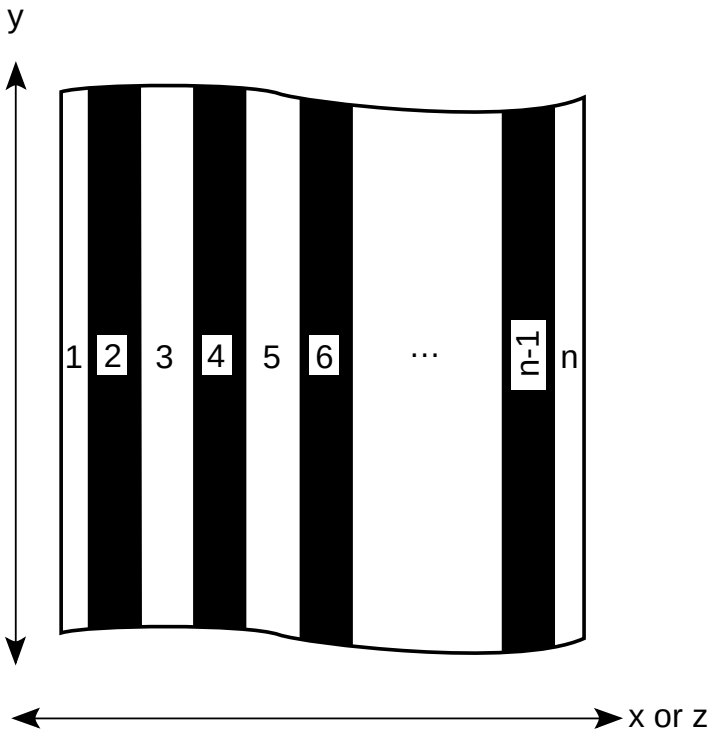

Fig. 2. The geometry of an n-layered (with n odd) unidirectional composite. The odd layers (in white) are matrix layers; the even layers (in black) are fiber layers. In an interlayer, shear-lag analysis, the fibers layers are assumed to be much stiffer than the matrix layers.

For the matrix layers, a second new assumption is that $v(x)$ is linear in x. It can then be expressed as a linear interpolation between $v(x_{i-1}) = \left\langle v^{(i-1)} \right\rangle$ and $v(x_i) = \left\langle v^{(i+1)} \right\rangle$. In dimensionless units

$$v^{(i)}(z_i) = \left\langle v^{(i-1)} \right\rangle (1 - z_i) + \left\langle v^{(i+1)} \right\rangle z_i \qquad \text{for } i \text{ odd} \tag{60}$$

Substituting these results into Hooke's law for shear stresses and making use of the fundamental shear-lag assumption leads to

$$\tau_{xy}^{(i)} = 0 \qquad \text{for } i \text{ even} \tag{61}$$

$$\tau_{xy}^{(i)} = \frac{G_{xy}^{(i)}}{t_i} \left(\left\langle v^{(i+1)} \right\rangle - \left\langle v^{(i-1)} \right\rangle \right) \qquad \text{for } i \text{ odd} \tag{62}$$

As derived here, it is seen that a Hedgepeth-type analysis satisfies continuity in axial displacement between layers ($v(x)$ is continuous). There are discontinuities, however, in shear stress at each fiber/matrix interface. Because this analysis requires that the stiff fibers be separated by soft matrix interlayers, we denote a Hedgepeth-type analysis as an *interlayer, shear-lag analysis*. It is clearly less accurate than the optimal, shear-lag analysis which correctly satisfies continuity in both axial displacements and shear stresses at all layer interfaces. From the interlayer analysis assumptions, its accuracy will approach the optimal, shear-lag analysis as the stiffness ratio between the stiff and soft layers approaches infinity.

The equations for an interlayer, shear-lag analysis can be derived by substituting eq. (31) into eq. (62). The method is similar to the derivation of the optimal, shear-lag equations. If we define $\boldsymbol{\tau}_I = (\tau_{xy}^{(3)}, \ldots, \tau_{xy}^{(n-2)})$ to be a vector of the constant shear stresses in the internal interlayers, the equation for the shear stresses is

$$[A_I] \frac{d^2 \boldsymbol{\tau}_I}{dy^2} - [B_I] \boldsymbol{\tau}_I = -\boldsymbol{\tau}_{I,0} \tag{63}$$

where $[A_I]$ is an $(n-3)/2 \times (n-3)/2$ diagonal matrix with the i^{th} diagonal element being

$$(A_I)_{i,i} = \frac{t_{2i+1}}{G_{xy}^{(2i+1)}} \tag{64}$$

and $[B_I]$ is an $(n-3)/2 \times (n-3)/2$ version $[B]$ in eq. (35) except it uses only the moduli and thicknesses of the stiff layers:

$$(B_I)_{i,i-1} = -\frac{1}{E_y^{(2i)}t_{2i}}, \quad (B_I)_{i,i} = \frac{1}{E_y^{(2(i+1))}t_{2(i+1)}} + \frac{1}{E_y^{(2i)}t_{2i}}, \quad \text{and} \quad (B_I)_{i,i+1} = -\frac{1}{E_y^{(2(i+1))}t_{2(i+1)}} \tag{65}$$

The vector $\boldsymbol{\tau}_{I,0}$ allows the interlayer, shear-lag analysis to account for non-zero shear stress boundary conditions. It is defined by

$$\boldsymbol{\tau}_0 = \left(\frac{\tau_{xy}^{(1)}}{E_y^{(2)}t_2}, 0, \ldots, \frac{\tau_{xy}^{(n)}}{E_y^{(n-1)}t_{n-1}} \right) \tag{66}$$

The interlayer, shear-lag equation for interlayer, shear stresses can be transformed to alternate forms by methods identical to those used in the optimal, shear-lag analysis. The shear stress equation can be written as

$$\frac{d^2\boldsymbol{\tau}_I}{dy^2} - [M_{I,\tau}]\boldsymbol{\tau}_I = -[M_{I,\tau}]\boldsymbol{\tau}_{I,\infty} \tag{67}$$

where $[M_{I,\tau}] = [A_I]^{-1}[B_I]$ and $\boldsymbol{\tau}_{I,\infty} = [B_I]^{-1}\boldsymbol{\tau}_{I,0}$ or

$$(\boldsymbol{\tau}_{I,\infty})_i = \tau_{xy}^{(1)} + \sum_{j=2,4}^{2i} \frac{t_j E_y^{(j)}}{t_I E_{I,y}^0}(\tau_n - \tau_0) \tag{68}$$

Here, $t_I = \sum_{i=2,4}^{n-1} t_i$ and $E_{I,y}^0$ only includes the contributions of the stiff layers:

$$E_{I,y}^0 = \frac{1}{t_I}\sum_{i=2,4}^{n-1} E_y^{(i)}t_i \tag{69}$$

A transformation to an equation for average axial stresses in the stiff layers can be derived by using

$$\boldsymbol{\tau}_I = \tau_{xy}^{(1)}(1,1,\ldots,1) - [I_L]\frac{d\mathbf{p}_I}{dy} \tag{70}$$

where $\mathbf{p}_I = (t_2\left\langle\sigma_y^{(2)}\right\rangle, t_4\left\langle\sigma_y^{(4)}\right\rangle, \ldots, t_{n-3}\left\langle\sigma_y^{(n-3)}\right\rangle)$ is a vector of net forces per unit plate depth in the stiff layers. The result is

$$\frac{d^2\mathbf{p}_I}{dy^2} - [M_{I,\sigma}]\mathbf{p} = -[M_{I,\sigma}]\mathbf{p}_{I,\infty} \tag{71}$$

where $[M_{I,\sigma}] = [I_L]^{-1}[A_I]^{-1}[B][I_L]$ and the i^{th} element of $\mathbf{p}_{I,\infty}$ is

$$(\mathbf{p}_{I,\infty})_i = t_{2i}E_y^{(2i)}\left[\frac{(\tau_{xy}^{(1)} - \tau_{xy}^{(n)})y + t_I\sigma_0(0)}{t_I E_{I,y}^0} + (\alpha_{I,y}^0 - \alpha_y^{(2i)})\Delta T\right] \tag{72}$$

Here $\alpha_{I,y}^0$ only includes the contributions of the stiff layers:

$$\alpha_{I,y}^0 = \sum_{i=2,4}^{n-1} \frac{\alpha_y^{(i)}t_i E_y^{(i)}}{t_I E_{I,y}^0} \tag{73}$$

Although interlayer, shear-lag analysis is less accurate than an optimal, shear-lag analysis, it has two important mathematical simplifications. First, an optimal, shear-lag analysis for n layers requires the solution of $n-1$ coupled differential equations, while the corresponding interlayer, shear-lag analysis has only $(n-3)/2$

equations. Second, the matrix $[M_\sigma]$ may be fully populated with non-zero elements. In contrast, because $[A_I]$ is diagonal, the matrix $[M_{I,\sigma}]$ is always tridiagonal. For analysis of a unidirectional composite in which all fiber layers have the same properties ($E_y^{(i)} = E_f$ and $t_i = d_f$) and all internal matrix layers have the same properties ($G_{xy}^{(i)} = G_m$ and $t_i = d_m$), $[M_{I,\sigma}]$ reduces to

$$[M_{I,\sigma}] = \frac{G_m}{E_f d_f d_m} \begin{bmatrix} 1 & -1 & 0 & 0 & \cdots \\ -1 & 2 & -1 & 0 & \cdots \\ 0 & -1 & 2 & -1 & \cdots \\ \vdots & \vdots & \vdots & \vdots & \vdots \\ \cdots & 0 & -1 & 2 & -1 \\ \cdots & 0 & 0 & -1 & 1 \end{bmatrix} \tag{74}$$

The eigenvalues and eigenvectors of this tridiagonal matrix in eq. (74) can be derived analytically which greatly simplifies the solution of the interlayer, shear-lag equations for unidirectional composites (Nairn, 1988a).

Parametric, Interlayer, Shear-Lag Analysis

Occasionally, Hedgepeth-type, interlayer, shear-lag models have been applied to multilayer composites in which the properties of the layers are different, but the stiffer layers are insufficiently stiffer than the more compliant layers to justify the requirements of an interlayer analysis. In some models, such a problem has been converted to an interlayer analysis by inserting fictitious interlayers between the actual layers with some shear modulus, $G_{xy}^{(int)}$, and thickness, t_{int} (Reifsnider, 1977; Laws and Dvorak, 1988; McManus and Maddocks, 1996). Such a structure is then amenable to an interlayer, shear-lag analysis. Because the inserted interlayers are fictitious, however, the interlayer properties are unknown parameters. Here, we denote such an analysis a *parametric, interlayer, shear-lag analysis*. Parametric, interlayer, shear-lag analysis is the least useful shear-lag method. The optimal, shear-lag and interlayer, shear-lag methods give explicit results for average axial stress and shear stress as a function of layer properties and thicknesses. In contrast, parametric, interlayer, shear-lag analysis only gives results that depend on unknown parameters. The parameters must be determined by fitting to experimental results. Parametric, interlayer, shear-lag analysis it is not actually a stress analysis method. It is better described as an empirical representation of the stresses that can be fit to experimental results. Because planar shear-lag methods are available that provide explicit stress-state solutions, parametric, interlayer, shear-lag analysis should only be used when optimal, shear-lag analysis is too complex and when the stiffnesses of the layers are too close to permit interlayer, shear-lag analysis.

3. Examples

Microcracked Laminates ($n = 2$)

Figure (3) shows an $[(S)/90_n]_s$ laminate where (S) denotes any supporting sublaminate. When such laminates are loaded in tension normal to the fibers in the 90° plies, those plies crack into periodic matrix microcracks. There has been much experimental work on microcracking and various stress analysis methods have been used to evaluate the effect of microcracking on the properties of the laminate. Two recent review articles in Nairn, 2000 and Nairn and Hu, 1994 cover the topic of matrix microcracking and give many references. Most early work on microcracking used shear-lag methods to analyze the stresses in the unit cell of damage between two microcracks as illustrated in Fig. 3 (Caslini, Zanotti, and O'Brien, 1987; Dharani and Tang, 1990; Flaggs, 1985; Garrett and Bailey, 1977; Han, Hahn, and Croman, 1987a; Han, Hahn, and Croman, 1987b; Laws and Dvorak, 1988; Manders, Chou, Jones, and Rock, 1983; McManus and Maddocks, 1996; Reifsnider, 1977; Tan and Nuismer, 1990). With the exception of McCartney (1992), however, shear-lag analyses of microcracking have used sub-optimal methods that suffer in accuracy. In this section, we use the results of the previous section to write down the *optimal* shear-lag analysis for a microcracked laminate and compare it to some prior shear-lag analyses of microcracked laminates.

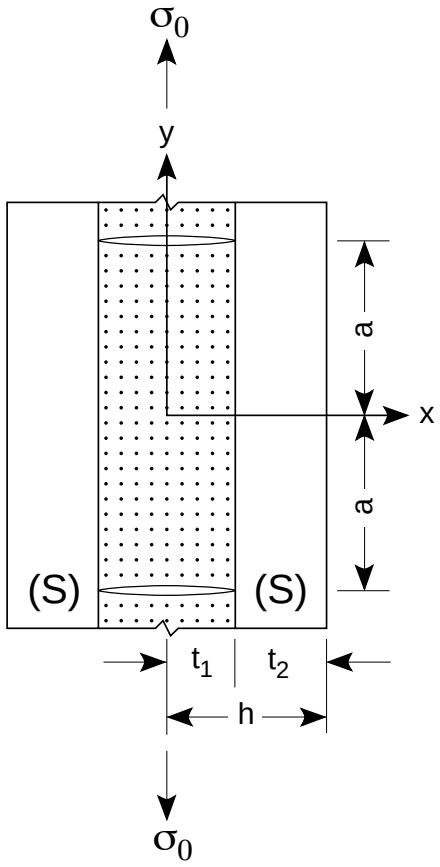

Fig. 3. A unit cell of damage between two microcracks located at $y = \pm a$ in a microcracked $[(S)/90_n]_s$ laminate. This figure has an edge view of the laminate. By symmetry, the stress analysis only needs to consider half the laminate which contains two layers. Layer 1 is the 90° plies; layer 2 is the (S) sublaminate.

Due to symmetry, the analysis of the microcracking unit cell reduces to an $n = 2$ problem with layer 1 being the 90° plies and layer 2 being the supporting plies. When $n = 2$, the system of second order equations in eq. (45) reduces to a single equation. The optimal, shear-lag equation is

$$\frac{d^2p_1}{dy^2} - \beta^2 p_1 = -\beta^2 p_{\infty,1} \tag{75}$$

where

$$\beta^2 = \frac{\dfrac{1}{E_y^{(1)}t_1} + \dfrac{1}{E_y^{(2)}t_2}}{\dfrac{t_1\langle z_1 R_1\rangle}{G_{xy}^{(1)}} + \dfrac{t_2\langle (1-z_2)L_2\rangle}{G_{xy}^{(2)}}} \tag{76}$$

Using boundary conditions that $p_1(\pm a) = 0$ on the microcrack surfaces, eq. (75) is easily solved to give

$$\left\langle \sigma_y^{(1)} \right\rangle = E_y^{(1)}\left[\frac{\sigma_0}{E_y^0} + (\alpha_y^0 - \alpha_y^{(1)})\Delta T\right]\left(1 - \frac{\cosh\beta y}{\cosh\beta a}\right) \tag{77}$$

From this (or any shear-lag) stress analysis, the effective, axial modulus of the laminate, E_y^*, in the presence of microcracks can be determined to be (Nairn and Hu, 1994; Nairn, 2000):

$$\frac{E_y^0}{E_y^*} = 1 + \frac{t_1E_y^{(1)}}{t_2E_y^{(2)}}\frac{\tanh\beta a}{\beta a} \tag{78}$$

The shear-lag equation for a microcracked laminate in eq. (75) was derived in many previous papers. Although the equation is the same, these previous papers differ in the value of the derived shear-lag parameter β. We claim the result in eq. (76) is the optimal, shear-lag parameter and that prior results with different β's are less accurate and should be abandoned. For example, two commonly-used microcracking shear-lag parameters are (Garrett and Bailey, 1977; Bailey, Curtis, and Parvizi, 1979):

$$\beta_1^2 = \frac{\frac{1}{E_y^{(1)}t_1} + \frac{1}{E_y^{(2)}t_2}}{\frac{t_1}{G_{xy}^{(1)}}} \qquad \text{and} \qquad \beta_2^2 = \frac{\frac{1}{E_y^{(1)}t_1} + \frac{1}{E_y^{(2)}t_2}}{\frac{t_1}{3G_{xy}^{(1)}}} \tag{79}$$

The first result reduces to the optimal result if $\langle z_1 R_1\rangle = 1$ and either $G_{xy}^{(2)} >> G_{xy}^{(1)}$ or $\langle (1-z_2)L_2\rangle = 0$; the second result if $\langle z_1 R_1\rangle = 1/3$ and either $G_{xy}^{(2)} >> G_{xy}^{(1)}$ or $\langle (1-z_2)L_2\rangle = 0$. These additional assumptions are not required; furthermore, for most laminate materials $G_{xy}^{(2)}$ is not much greater than $G_{xy}^{(1)}$. Several other papers have derived parametric, interlayer, shear-lag analyses (Reifsnider, 1977; Laws and Dvorak, 1988; McManus and Maddocks, 1996). Because these analyses introduce an unknown parameter into the shear-lag parameter, they are not useful as methods for making explicit predictions about stresses or effective modulus. Only McCartney has previously derived an optimal, shear-lag analysis of microcracking (McCartney, 1992). His shear-lag parameter is a special case of eq. (76) which assumes all shape functions are linear.

A sample calculation of modulus reduction for a microcracked $[0/90_2]_s$ E-Glass/Epoxy laminate is given in Fig. 4. The lines are shear-lag calculations with various shear-lag parameters; the symbols are finite element calculations. The shear-lag analyses using β_1 are β_2 are not accurate. The McCartney analysis, in contrast, is extremely accurate. It agrees with the finite element analyses with an accuracy of better than 0.54% for crack densities less than 0.9 mm^{-1} and 0.80% for the last crack density of 1.0 mm^{-1}. The shear-lag results can be slightly improved by adjusting the shape functions averages to $\langle z_1 R_1\rangle = 0.3300$ and $\langle (1-z_2)L_2\rangle = 0.3070$. The resulting curve, labeled "Optimized Shape Functions," agrees with finite element analysis with an accuracy of better than 0.20% for crack densities less than 0.9 mm^{-1} and 0.48% for the last crack density of 1.0 mm^{-1}. The improvement over the McCartney analysis, which assumes linear shape functions, is only marginal and probably not worth the effort of calculating the shape function averages by minimization of errors. Thus, if one must analyze microcracked laminates using shear-lag analysis, that analysis should be done in terms of the McCartney (1992) shear-lag parameter.

Although Fig. 4 shows that shear-lag analysis with linear shape functions can accurately predict modulus reduction in microcracked, cross-ply laminates, shear-lag analysis is less accurate when applied to calculating energy release rates for microcrack formation (Nairn, 2000; Nairn, Hu, and Bark, 1993; Nairn and Hu, 1994). Calculation of the energy release rate for microcracking requires evaluation of the change in modulus which is equivalent to finding the derivative of the effective modulus. Although shear-lag may be accurate for the modulus, it is less accurate for finding the derivative of the modulus. When shear-lag analysis is used with a fracture mechanics method for predicting the formation of microcracks in a variety of laminates, it gives results that are less accurate than two-dimensional stress analyses based on variational mechanics (Nairn, 2000; Nairn, Hu, and Bark, 1993; Nairn and Hu, 1994). Perhaps the shear-lag analysis could be improved by optimizing the shape function averages for each specific layup, but the variational mechanics results can analyze a wide range of layups without the need for optimizing any parameters (Nairn, 2000; Nairn, Hu, and Bark, 1993; Nairn and Hu, 1994).

Compression Double Lap Shear ($n = 3$)

A new double-lap shear specimen has recently been developed that consists of three equal-thickness metal adherends connected by two equal-thickness adhesive layers (Mendels, Page, Leterrier, Månson, and Nairn, 2000). This specimen is tested in compression by supporting the two outer metal plates and loading the central plate in compression until adhesive failure. By symmetry, a shear-lag analysis of this specimen only needs to consider half the specimen as illustrated in Fig. 5. The optimal, shear-lag analysis of this specimen is a three-layer problem or one more layer than the analysis of the microcracked specimen in the previous section.

The optimal, shear-lag equation for the average axial stresses in layers 1 and 2 is given in eq. (45) where

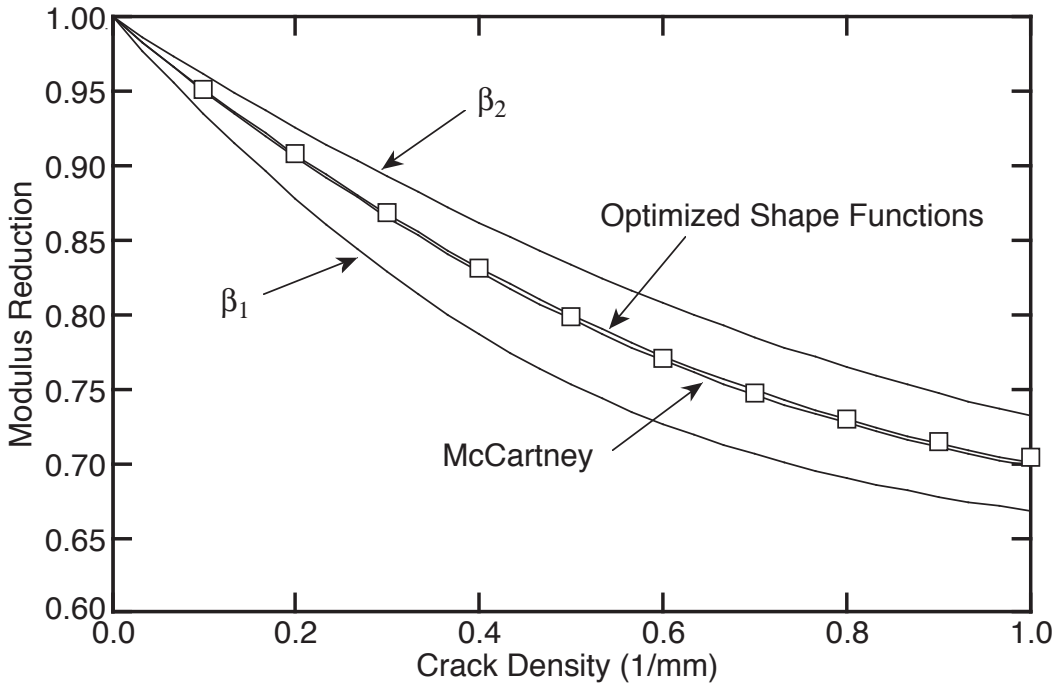

Fig. 4. Modulus reduction in an $[0/90_2]_s$ E-Glass/Epoxy laminate as a function of microcrack density calculated by various shear-lag models and compared to finite element analysis. For the sample calculations in this paper, $E_y^{(1)} = 13$ GPa, $G_{xy}^{(1)} = 4.58$ GPa, $t_1 = 0.42$ mm, $E_y^{(2)} = 41.7$ GPa, $G_{xy}^{(2)} = 3.4$ GPa, and $t_2 = 0.21$ mm.

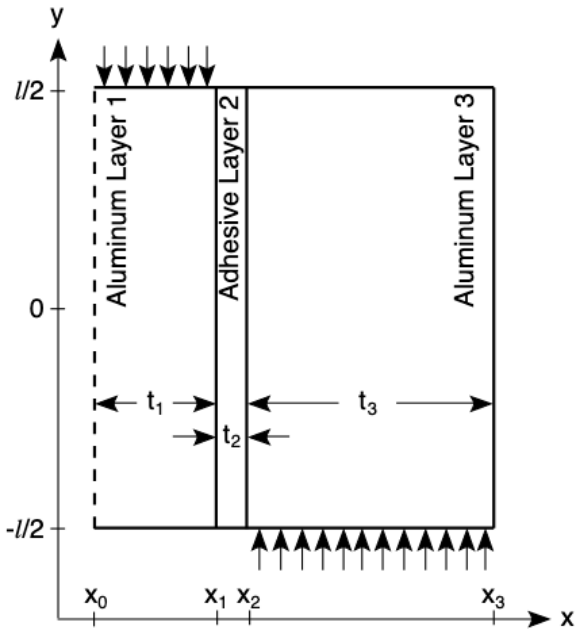

Fig. 5. The right half of a compression double-lap shear specimen. For the sample calculations in this paper, the two Aluminum layers have $E_y^{(i)} = 69000$ MPa and $\nu_{xy}^{(i)} = 0.25$, $t_1 = 2$ mm, and $t_3 = 4$ mm. The adhesive layer has $E_y^{(2)} = 3167$ MPa, $\nu_{xy}^{(2)} = 0.33$, and $t_2 = 0.15$ mm. The total specimen length is $l = 20$ mm.

matrix $[M_\sigma]$ is derived from the $[A]$ and $[B]$ matrices

$$[A] = \begin{pmatrix} \dfrac{t_1\langle z_1R_1\rangle}{G_{xy}^{(1)}} + \dfrac{t_2\langle(1-z_2)L_2\rangle}{G_{xy}^{(2)}} & \dfrac{t_2\langle(1-z_2)R_2\rangle}{G_{xy}^{(2)}} \\ \dfrac{t_2\langle z_2L_2\rangle}{G_{xy}^{(2)}} & \dfrac{t_2\langle z_2R_2\rangle}{G_{xy}^{(2)}} + \dfrac{t_3\langle(1-z_3)L_3\rangle}{G_{xy}^{(3)}} \end{pmatrix} \tag{80}$$

$$[B] = \begin{pmatrix} \dfrac{1}{E_y^{(1)}t_1} + \dfrac{1}{E_y^{(2)}t_2} & -\dfrac{1}{E_y^{(2)}t_2} \\ -\dfrac{1}{E_y^{(2)}t_2} & \dfrac{1}{E_y^{(2)}t_2} + \dfrac{1}{E_y^{(3)}t_3} \end{pmatrix} \tag{81}$$

(82)

We consider a specimen with unit compression on the top of layer 1 ($\sigma_0(0) = -t_1/t$), zero shear stresses on the lateral surfaces ($\tau_0 = \tau_n = 0$), and zero residual stresses ($\Delta T = 0$, note: it is straightforward to add residual stresses if they occur in the adhesive specimen). Using eq. (48), the average axial stresses in the layers are:

$$\left\langle\sigma_y^{(1)}\right\rangle = -\frac{t_1E_y^{(1)}}{tE_y^0} + \left(a_1e^{\lambda_1y} + b_1e^{-\lambda_1y}\right)\frac{\psi_{1,1}}{t_1} + \left(a_2e^{\lambda_2y} + b_2e^{-\lambda_2y}\right)\frac{\psi_{2,1}}{t_1} \tag{83}$$

$$\left\langle\sigma_y^{(2)}\right\rangle = -\frac{t_1E_y^{(2)}}{tE_y^0} + \left(a_1e^{\lambda_1y} + b_1e^{-\lambda_1y}\right)\frac{\psi_{1,2}}{t_2} + \left(a_2e^{\lambda_2y} + b_2e^{-\lambda_2y}\right)\frac{\psi_{2,2}}{t_2} \tag{84}$$

$$\left\langle\sigma_y^{(3)}\right\rangle = -\frac{t_1E_y^{(3)}}{tE_y^0} - \left(a_1e^{\lambda_1y} + b_1e^{-\lambda_1y}\right)\frac{\psi_{1,1}+\psi_{1,2}}{t_3} - \left(a_2e^{\lambda_2y} + b_2e^{-\lambda_2y}\right)\frac{\psi_{2,1}+\psi_{2,2}}{t_3} \tag{85}$$

where λ_1 and λ_2 are the two eigenvalues of $[M_\sigma]$ with eigenvectors $(\psi_{1,1}, \psi_{1,2})$ and $(\psi_{2,1}, \psi_{2,2})$. Using eq. (49), the interfacial shear stresses at the two interfaces between the adherends and the adhesive are

$$\tau(x_1) = -\left(a_1e^{\lambda_1y} - b_1e^{-\lambda_1y}\right)\lambda_1\psi_{1,1} - \left(a_2e^{\lambda_2y} - b_2e^{-\lambda_2y}\right)\lambda_2\psi_{2,1} \tag{86}$$

$$\tau(x_2) = -\left(a_1e^{\lambda_1y} - b_1e^{-\lambda_1y}\right)\lambda_1(\psi_{1,1}+\psi_{1,2}) - \left(a_2e^{\lambda_2y} - b_2e^{-\lambda_2y}\right)\lambda_2(\psi_{2,1}+\psi_{2,2}) \tag{87}$$

By integrating a one-dimensional Hooke's law (eq. (32) with $\Delta T = 0$ in this example), the average axial displacement in each layer is

$$\left\langle v^{(i)}\right\rangle = \left\langle v^{(i)}(-l/2)\right\rangle + \int_{-l/2}^{l/2}\frac{\left\langle\sigma_y^{(i)}\right\rangle}{E_y^{(i)}}dy \tag{88}$$

Doing the integrations, setting $\left\langle v^{(3)}(-l/2)\right\rangle = 0$ at the supported base of the specimen, and making use of eq. (26) at $y = -l/2$ results in

$$\begin{aligned}\left\langle v^{(1)}\right\rangle = &-\left(\frac{t_1\langle z_1R_1\rangle}{G_{xy}^{(1)}} + \frac{t_2\langle L_2\rangle}{G_{xy}^{(2)}}\right)\tau\left(x_1,-\frac{l}{2}\right) - \left(\frac{t_3\langle(1-z_3)L_3\rangle}{G_{xy}^{(3)}} + \frac{t_2\langle R_2\rangle}{G_{xy}^{(2)}}\right)\tau\left(x_2,-\frac{l}{2}\right) - \frac{t_1(y+\frac{l}{2})}{tE_y^0} \\ &+ \left[a_1\left(e^{\lambda_1y} - e^{-\lambda_1\frac{l}{2}}\right) + b_1\left(e^{\lambda_1\frac{l}{2}} - e^{-\lambda_1y}\right)\right]\frac{\psi_{1,1}}{\lambda_1E_y^{(1)}t_1} \\ &+ \left[a_2\left(e^{\lambda_2y} - e^{-\lambda_2\frac{l}{2}}\right) + b_2\left(e^{\lambda_2\frac{l}{2}} - e^{-\lambda_2y}\right)\right]\frac{\psi_{2,1}}{\lambda_2E_y^{(1)}t_1}\end{aligned} \tag{89}$$

$$\begin{aligned}\left\langle v^{(2)}\right\rangle = &-\frac{t_2\langle z_2L_2\rangle}{G_{xy}^{(2)}}\tau\left(x_1,-\frac{l}{2}\right) - \left(\frac{t_3\langle(1-z_3)L_3\rangle}{G_{xy}^{(3)}} + \frac{t_2\langle z_2R_2\rangle}{G_{xy}^{(2)}}\right)\tau\left(x_2,-\frac{l}{2}\right) - \frac{t_1(y+\frac{l}{2})}{tE_y^0} \\ &+ \left[a_1\left(e^{\lambda_1y} - e^{-\lambda_1\frac{l}{2}}\right) + b_1\left(e^{\lambda_1\frac{l}{2}} - e^{-\lambda_1y}\right)\right]\frac{\psi_{1,2}}{\lambda_1E_y^{(2)}t_2} \\ &+ \left[a_2\left(e^{\lambda_2y} - e^{-\lambda_2\frac{l}{2}}\right) + b_2\left(e^{\lambda_2\frac{l}{2}} - e^{-\lambda_2y}\right)\right]\frac{\psi_{2,2}}{\lambda_2E_y^{(2)}t_2}\end{aligned} \tag{90}$$

$$\left\langle v^{(3)}\right\rangle = -\frac{t_1(y+\frac{l}{2})}{tE_y^0} - \left[a_1\left(e^{\lambda_1 y} - e^{-\lambda_1\frac{l}{2}}\right) - b_1\left(e^{\lambda_1\frac{l}{2}} - e^{-\lambda_1 y}\right)\right]\frac{\psi_{1,1}+\psi_{1,2}}{\lambda_1 E_y^{(3)} t_3} - \left[a_2\left(e^{\lambda_2 y} - e^{-\lambda_2\frac{l}{2}}\right) + b_2\left(e^{\lambda_2\frac{l}{2}} - e^{-\lambda_2 y}\right)\right]\frac{\psi_{2,1}+\psi_{2,2}}{\lambda_2 E_y^{(3)} t_3} \tag{91}$$

Finally, the energy in the specimen can be calculated by a boundary integral of tractions and displacements to be

$$U = \frac{Wt_1}{2}\left\langle\sigma_y^{(1)}(l/2)\right\rangle\left\langle v^{(1)}(l/2)\right\rangle \tag{92}$$

where W is the width of the specimen in the z direction. From eq. (89) and $\left\langle\sigma_y^{(1)}(l/2)\right\rangle = -1$, the energy is

$$U = \frac{Wt_1}{2}\left[\left(\frac{t_1\langle z_1 R_1\rangle}{G_{xy}^{(1)}} + \frac{t_2\langle L_2\rangle}{G_{xy}^{(2)}}\right)\tau\left(x_1, -\frac{l}{2}\right) + \left(\frac{t_3\langle(1-z_3)L_3\rangle}{G_{xy}^{(3)}} + \frac{t_2\langle R_2\rangle}{G_{xy}^{(2)}}\right)\tau\left(x_2, -\frac{l}{2}\right) + \frac{t_1 l}{tE_y^0} - \frac{2(a_1+b_1)\psi_{1,1}}{\lambda_1 E_y^{(1)} t_1}\sinh\frac{\lambda_1 l}{2} - \frac{2(a_2+b_2)\psi_{2,1}}{\lambda_2 E_y^{(1)} t_1}\sinh\frac{\lambda_2 l}{2}\right] \tag{93}$$

Because the adhesive layer is thin compared to the other layers, it is probably accurate to use linear shape functions in the adhesive layer ($L_2 = 1 - z_2$ and $R_2 = z_2$). With this assumption, the shear stresses in layer 2 are linear in the x direction. Thus, the average shear stress in the adhesive layer is

$$\left\langle\tau_{xy}^{(2)}\right\rangle = -\frac{1}{2}\left[\left(a_1 e^{\lambda_1 y} - b_1 e^{-\lambda_1 y}\right)\lambda_1(2\psi_{1,1}+\psi_{1,2}) + \left(a_2 e^{\lambda_2 y} - b_1 e^{-\lambda_2 y}\right)\lambda_2(2\psi_{2,1}+\psi_{2,2})\right] \tag{94}$$

The remaining shape functions, R_1 and L_3, may or may not be linear. Several possibilities for these shape functions will be considered below. Finally, the four unknown constants, a_1, b_1, a_2, and b_2, can be found by satisfying the four axial-stress boundary conditions

$$\left\langle\sigma_y^{(1)}(+l/2)\right\rangle = -1, \quad \left\langle\sigma_y^{(1)}(-l/2)\right\rangle = 0, \quad \left\langle\sigma_y^{(2)}(+l/2)\right\rangle = 0, \quad \text{and} \quad \left\langle\sigma_y^{(2)}(-l/2)\right\rangle = 0 \tag{95}$$

Because the adhesive layer is thin relative to the adherend layers and has a much lower modulus, it is possible that an interlayer, shear-lag analysis will give results similar to the optimal, shear-lag analysis. If we imagine two phantom soft layers to the left of layer 1 and to the right or layer 3, the interlayer, shear-lag equation in eq. (71) reduces to a single equation:

$$\frac{d^2\left\langle\sigma_y^{(1)}\right\rangle}{dy^2} - \alpha^2\left\langle\sigma_y^{(1)}\right\rangle = \alpha^2\frac{t_1 E_y^{(1)}}{t_I E_{I,y}^0} \tag{96}$$

where $t_I = t_1 + t_3$, $E_{I,y}^0 = (t_1 E_y^{(1)} + t_3 E_y^{(3)})/t_I$, and

$$\alpha^2 = \frac{G_{xy}^{(2)}}{t_2}\left(\frac{1}{E_y^{(1)} t_1} + \frac{1}{E_y^{(3)} t_3}\right) \tag{97}$$

For better comparison with the optimal, shear-lag analysis, the phantom layer to the left of layer 1 is called layer 0. Now, the odd layers are the stiff layers and the even layers are the interlayers. Making use of the first two boundary conditions in eq. (95) and noting that $E_y^{(1)} = E_y^{(3)}$ in this specimen, the interlayer, shear-lag solution is

$$\left\langle\sigma_y^{(1)}\right\rangle = \frac{(t_1-t_3)\sinh\alpha\frac{l}{2}\cosh\alpha y - t_I\cosh\alpha\frac{l}{2}\sinh\alpha y - t_1\sinh\alpha l}{t_I\sinh\alpha l} \tag{98}$$

$$\left\langle\sigma_y^{(3)}\right\rangle = -\frac{t_1}{t_3}\left[\frac{(t_1-t_3)\sinh\alpha\frac{l}{2}\cosh\alpha y - t_I\cosh\alpha\frac{l}{2}\sinh\alpha y + t_3\sinh\alpha l}{t_I\sinh\alpha l}\right] \tag{99}$$

Making use of eq. (28), the average shear stress in the adhesive interlayer is

$$\left\langle \tau_{xy}^{(2)} \right\rangle = -t_1\alpha \left[\frac{(t_1-t_3)\sinh\alpha\frac{l}{2}\sinh\alpha y - t_I\cosh\alpha\frac{l}{2}\cosh\alpha y}{t_I\sinh\alpha l} \right] \tag{100}$$

By integrating a one-dimensional Hooke's law, setting $\left\langle v^{(3)}(-l/2)\right\rangle = 0$ at the supported base of the specimen, and making use of eq. (62) at $y=-l/2$, the average displacements in the two stiff layers are

$$\begin{aligned} \left\langle v^{(1)} \right\rangle &= -\frac{t_2}{G_{xy}^{(2)}}\left\langle \tau_{xy}^{(2)}\left(-\frac{l}{2}\right)\right\rangle + \frac{1}{t_I E_{I,y}^0}\left[\frac{(t_1-t_3)\sinh\alpha\frac{l}{2}(\sinh\alpha y+\sinh\alpha\frac{l}{2})}{\alpha\sinh\alpha l}\right. \\ &\qquad \left. -\frac{t_I\cosh\alpha\frac{l}{2}(\cosh\alpha y-\cosh\alpha\frac{l}{2})}{\alpha\sinh\alpha l} - t_1\left(y+\frac{l}{2}\right)\right] \end{aligned} \tag{101}$$

$$\begin{aligned} \left\langle v^{(3)} \right\rangle &= -\frac{t_1}{t_3 t_I E_{I,y}^0}\left[\frac{(t_1-t_3)\sinh\alpha\frac{l}{2}(\cosh\alpha y-\cosh\alpha\frac{l}{2})}{\alpha\sinh\alpha l}\right. \\ &\qquad \left. -\frac{t_I\cosh\alpha\frac{l}{2}(\sinh\alpha y+\sinh\alpha\frac{l}{2})}{\alpha\sinh\alpha l} + t_3\left(y+\frac{l}{2}\right)\right] \end{aligned} \tag{102}$$

Finally, using a boundary integral of tractions and displacements, total energy in the specimen is

$$U_I = \frac{Wt_1}{2}\left[\frac{t_2}{G_{xy}^{(2)}}\left\langle \tau_{xy}^{(2)}\left(-\frac{l}{2}\right)\right\rangle + \frac{t_1 l}{t_I E_{I,y}^0} - \frac{(t_1-t_3)\tanh\alpha\frac{l}{2}}{\alpha t_I E_{I,y}^0}\right] \tag{103}$$

Figure (6) gives sample results for stresses in a double lap-shear specimen with aluminum adherends and an epoxy adhesive. The mechanical properties assumed for the aluminum and epoxy and the dimensions of the specimen are given in the caption to Fig. 5. These first calculations assumed linear shape functions or $\langle z_1 R_1\rangle = \langle (1-z_3)L_3\rangle = 1/3$. The plot includes calculations by an optimal, shear-lag analysis and by an interlayer, shear-lag analysis. These two results are compared to finite element calculations (FEA). For better comparison to FEA results, the FEA stresses were averaged over the thickness of the layers. For this specimen properties and geometry, both shear-lag analyses agree reasonably well with FEA results. As expected, the optimal, shear-lag analysis was always more accurate than the interlayer, shear-lag analysis. Both shear-lag analyses gave non-zero shear stress at $y=\pm l/2$. Because there is no applied shear stress on the specimen ends, the end shear-stress should approach zero. The FEA results tended towards zero at the ends, but they showed high shear-stress peak very close to the ends. The shear-lag results were good for shear stress with the exception of the small zone near the ends.

By adjusting the shape functions in the optimal, shear-lag analysis, it was possible to improve agreement between that analysis and FEA results. For any particular value selected for $\langle z_1 R_1\rangle$, we found that the best agreement with FEA results was obtained when $\langle (1-z_3)L_3\rangle$ was approximately twice as large as $\langle z_1 R_1\rangle$. This ratio is similar to the thickness ratio between layers three and one from the specimen analyzed (see Fig. 5). Closer inspection revealed that the optimum $\langle (1-z_3)L_3\rangle$ to $\langle z_1 R_1\rangle$ ratio was very closely equal to the stiffness ratio of layer three to the other two layers combined:

$$\left(\frac{\langle (1-z_3)L_3\rangle}{\langle z_1 R_1\rangle}\right)_{\text{Best Fit}} = \frac{E_y^{(3)}t_3}{E_y^{(1)}t_1 + E_y^{(2)}t_2} \tag{104}$$

This ratio is close to two because $t_3 = 2t_1$, $E_y^{(3)} = E_y^{(1)}$, and $E_y^{(2)}t_2$ is small compared to $E_y^{(1)}t_1$. Fixing the above shape function ratio, the optimal, shear-lag analysis can be matched to various features of the FEA results. Figure (7) is the result of adjusting the shape function to match the average axial stress in the adherend layers to the FEA results. The best-fit shape functions were $\langle z_1 R_1\rangle = 0.506$ and $\langle (1-z_3)L_3\rangle = 1.009$. With these shape functions, the optimal, shear-lag analysis for axial stresses was effectively identical to the FEA results. The shear-lag shear stress was also very close to the FEA results except for a small region near the specimen ends.

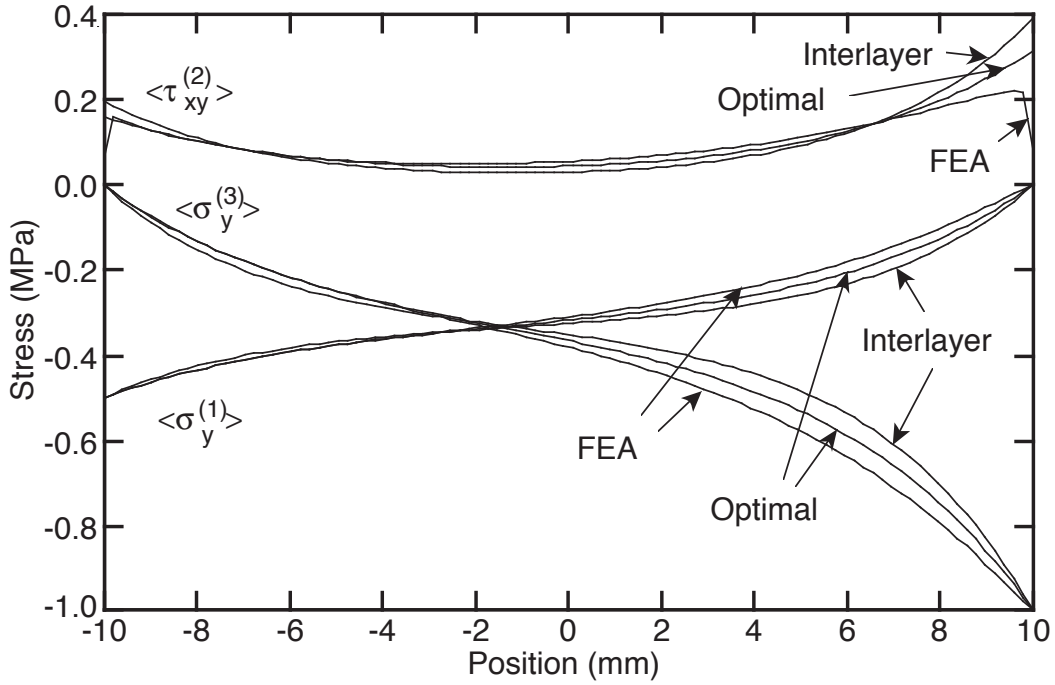

Fig. 6. The average tensile stresses in the Aluminum adherends and the average shear stress in the epoxy adhesive as a function of position in the specimen. The three plots for each result are for an optimal, shear-lag analysis with linear shape functions, an interlayer, shear-lag analysis, and finite element analysis.

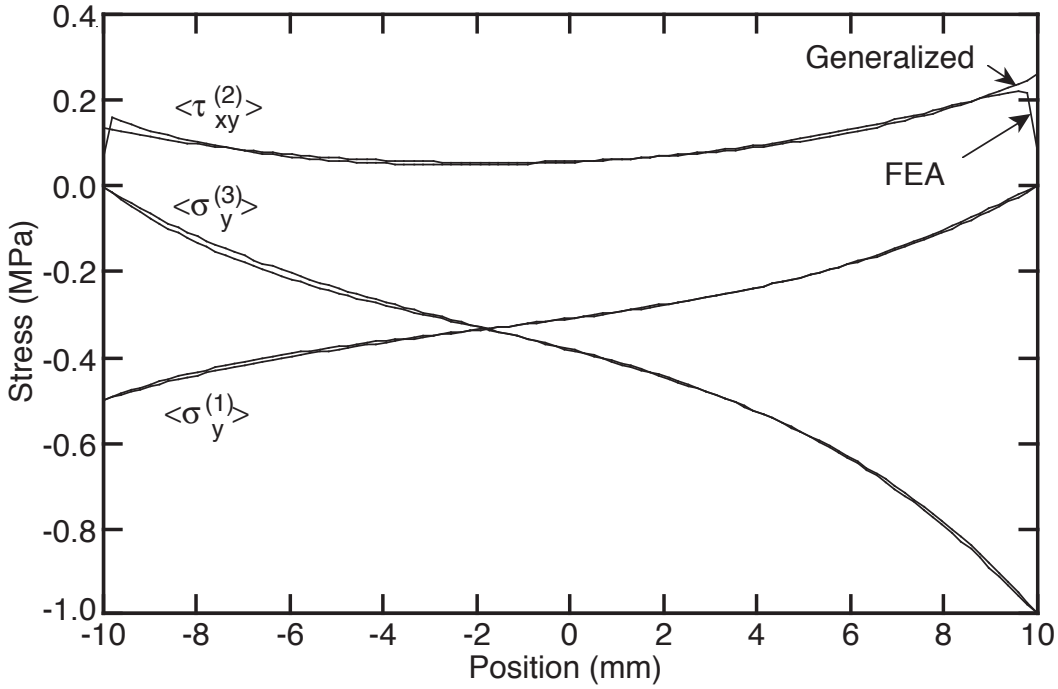

Fig. 7. The average tensile stresses in the Aluminum adherends and the average shear stress in the epoxy adhesive as a function of position in the specimen. The two plots for each result are for an optimal, shear-lag analysis with "best-fit" shape functions and finite element analysis.

When the displacements from an optimal, shear-lag analysis using shape functions adjusted to match FEA stresses were compared to FEA results for displacement and energy, it was found that optimizing the results to match stresses comes at the expense of getting worse results for displacement and therefore for energy. The shear-lag analysis could be adjusted to fit the FEA displacement almost exactly by using shape functions (still in the same ideal ratio) of $\langle z_1 R_1\rangle = 0.284$ and $\langle (1-z_3)L_3\rangle = 0.566$, but these shape functions led to worse results for axial stress. The trade off between fitting stresses and displacements is caused by the shear-lag displacement being calculated from a one-dimensional Hooke's law that ignores transverse stresses (see eq. (32)). If the shear-lag analysis is adjusted to match axial stresses, then the axial displacement will be in error by the consequence of ignoring transverse stresses. Similarly, if the shear-lag analysis is adjusted to match displacements, the error in axial stresses will reflect the magnitude of the error caused by ignoring transverse stresses. We suggest that a good *compromise* method is to adjust the shear-lag analysis to match the FEA results for energy. Because energy is a product of stresses and displacement (see eq. (92)), this approach gives a compromised, simultaneous fit to stresses and displacement. For this specific double-lap-shear specimen, the total energy in the shear-lag analysis matched the total energy in the FEA results when the shape functions were $\langle z_1 R_1\rangle = 0.317$ and $\langle (1-z_3)L_3\rangle = 0.632$.

Some more variations in the shape function parameters showed that the optimal, shear-lag analysis reduces to the interlayer, shear-lag analysis as $\langle z_1 R_1\rangle$ and $\langle (1-z_3)L_3\rangle$ approach zero. Physically, an interlayer, shear-lag analysis assumes there is zero shear stress in the stiff layers. Zero shear stress translates into shape functions averages equal to zero. Clearly, forcing the shear stresses in some layers to be zero is a much more restrictive assumption than letting them vary according to some shape functions. In other words, the interlayer, shear-lag analysis is always less accurate than the optimal, shear-lag analysis.

The previous results were all for a high modulus ratio between the adherend and the adhesive. The results in Fig. 8 are for the same specimen except the modulus of the adhesive was increased to be identical to the adherends. The small Poisson-ratio mismatch between the adhesive and the adherends was not changed. The optimal, shear-lag results in this analysis were adjusted to match the energy of the FEA results. The best-fit shape functions were $\langle z_1 R_1\rangle = 0.317$ and $\langle (1-z_3)L_3\rangle = 1/3 = 0.590$; $\langle z_1 R_1\rangle$ was identical to the previous result and $\langle (1-z_3)L_3\rangle$ again followed the stiffness ratio in eq. (104). Despite the dramatic change in modulus ratio, the optimal, shear-lag analysis still agrees well with FEA results. In contrast, the interlayer method breaks down. The interlayer, shear-lag analysis grossly overestimates the shear stress near the specimen ends. As a consequence, it also does a poor job of calculating axial stress transfer between layers one and three.

Unidirectional Composite ($n > 3$)

For an example with many layers, we analyzed a unidirectional composite with 5 fibers (see Fig. 2 with $n = 11$). The fiber layers had properties $t_i = t_f$, $E_y^{(i)} = E_f$, and $G_{xy}^{(i)} = G_f$. The matrix layers had properties $t_i = t_m$, $E_y^{(i)} = E_m$, and $G_{xy}^{(i)} = G_m$. The thickness of the first and last matrix layers were taken as $t_m/2$ to make the fiber volume fraction equal to $V_f = t_f/(t_f + t_m)$. We analyzed a sample of length $2L$ extending from $y = -L$ to $y = +L$. The sample was axially loaded on the ends with fiber stress $\left\langle \sigma_y^{(f)} \right\rangle = 1$ and matrix stress $\left\langle \sigma_y^{(m)} \right\rangle = E_m/E_f$. The total axial load was thus $\sigma_0 = E_y^0/E_f$. The thermal load ($\Delta T = 0$) and the transverse shear loads ($\tau_0 = \tau_{11} = 0$) were both taken to be zero although it would be trivial to include such loadings. A crack was introduced at $y = 0$ by breaking some layers. The broken layers had zero stress at $y = 0$; the intact layers had zero displacement at $y = 0$. Specifically, we always assumed the first two fiber and matrix layers were broken ($i = 1$ to 4) and considered problems where the next matrix layer ($i = 5$) was either intact or broken. For each problem analyzed, we looked at the stresses in the first unbroken fiber (fiber 3 or layer $i = 6$). Finally, the specimen dimensions were $L = 40$ mm and total width $5(t_f + t_m) = 10$ mm. Some calculations were done for $V_f = 0.5$ ($t_f = t_m = 1$). Some calculations varied V_f by varying the ratio of t_f to t_m while keeping their sum, and thus the specimen width, constant.

The system of equations for determining all layer axial stresses is given in eq. (45). The $[A]$ and $[B]$ matrices required for finding $[M_\sigma]$ are given in eq. (35) using the alternating layer properties given above. The eigenvalues and eigenvectors of $[M_\sigma]$ or $[M_\tau]$ were found as described in the *Solution Methods and Properties* section. The axial stresses in the layers were then given by eq. (48). The twenty unknown constants (a_j and b_j for $j = 1$ to 10) were determined from the following twenty boundary conditions. From

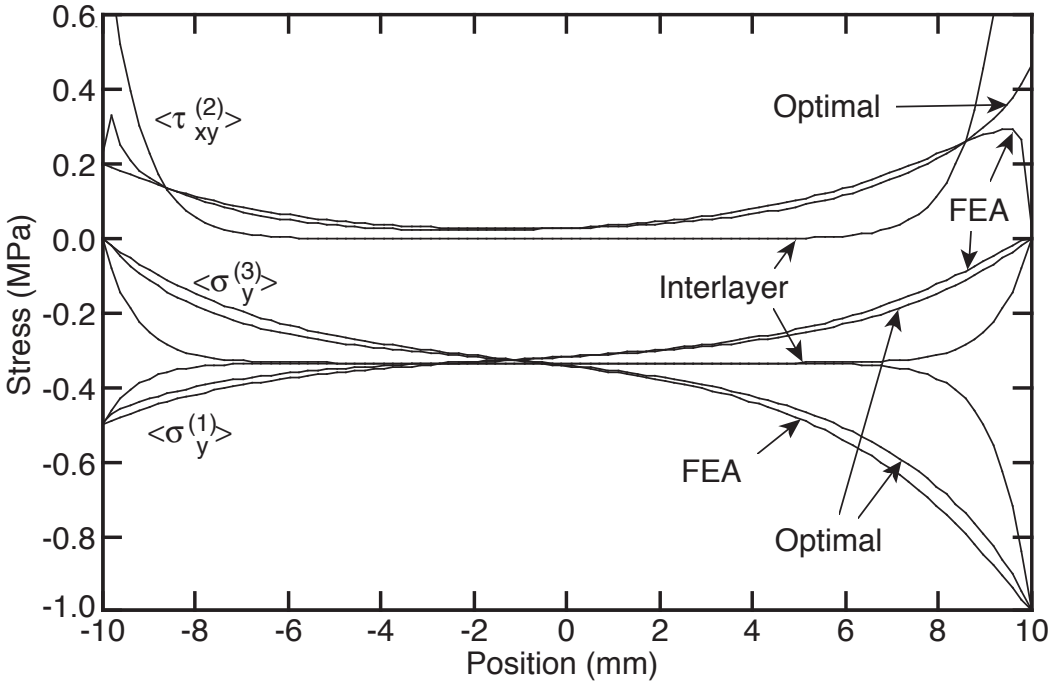

Fig. 8. The average tensile stresses in the Aluminum adherends and the average shear stress in an adhesive with the same modulus as the adherends as a function of position in the specimen. The three plots for each result are for an optimal, shear-lag analysis with shape functions optimized to match energy, an interlayer, shear-lag analysis, and finite element analysis.

the fiber and matrix loads on the end of the specimen:

$$\sum_{j=1}^{10}\left(a_j e^{\lambda_j L}+b_j e^{-\lambda_j L}\right)\frac{\psi_{j,i}}{t_i}=0 \qquad \text{for } i=1 \text{ to } 10 \tag{105}$$

When the first n_b layers are broken, the zero axial stress at $y=0$ in those layers gives the following boundary conditions:

$$\sum_{j=1}^{n-1}(a_j+b_j)\frac{\psi_{j,i}}{t_i}=\begin{cases}-\dfrac{E_m}{E_f} & i \text{ odd (matrix layers)}\\ -1 & i \text{ even (fiber layers)}\end{cases} \qquad \text{for } i=1 \text{ to } n_b \tag{106}$$

The unbroken fibers have zero displacement at $y=0$. These boundary conditions were set by setting the last-layer, $y=0$ displacement to be zero ($\langle v_{11}(0)\rangle=0$) and then using eq. (26) for each remaining unbroken layer. The resulting equations are:

$$\sum_{j=1}^{n-1}(a_j-b_j)\left[\frac{t_{i+1}}{G_{xy}^{(i+1)}}\left(\langle(1-z_{i+1})R_{i+1}\rangle\,\omega_{j,i+1}+\langle(1-z_{i+1})L_{i+1}\rangle\,\omega_{j,i}\right)\right. \tag{107}$$
$$\left.+\frac{t_i}{G_{xy}^{(i)}}\left(\langle z_i R_i\rangle\,\omega_{j,i}+\langle z_i L_i\rangle\,\omega_{j,i-1}\right)\right]=0 \qquad \text{for } i=n_b+1 \text{ to } 10$$

To make this equation work for $i=n-1=10$, we set $\omega_{j,11}=0$. Numerically solving the boundary condition equations had scaling problems because the a_j and b_j constants differed by many orders of magnitude. The scaling problems could be eliminating by replacing the a_j constants by new constants c_j defined by

$$c_j=a_j e^{\lambda_j L} \tag{108}$$

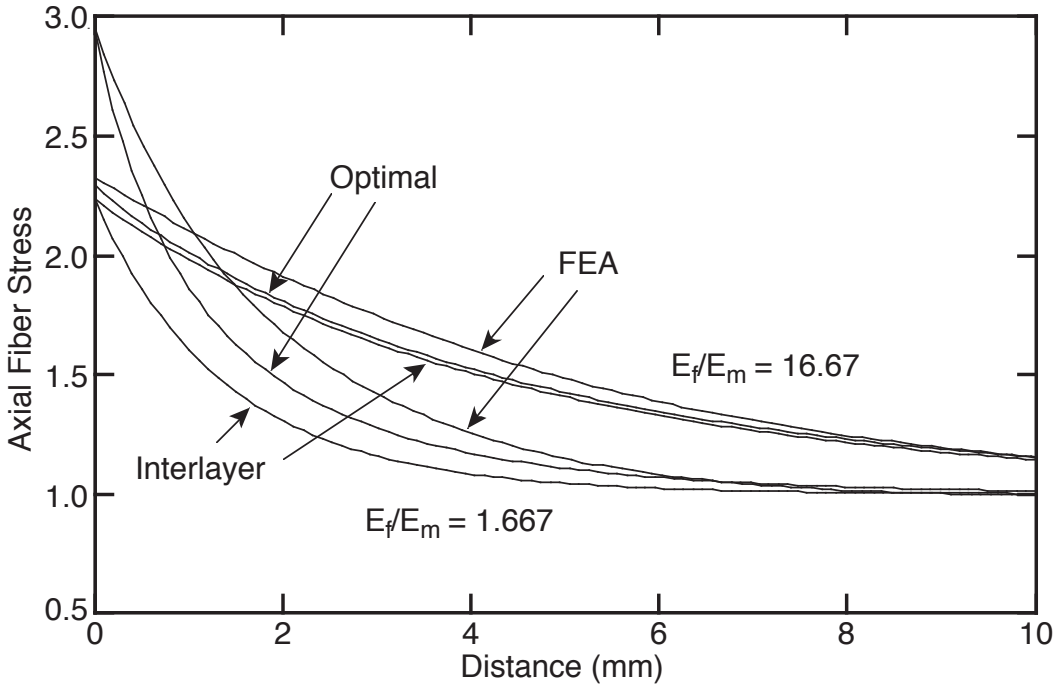

Fig. 9. The average axial fiber stress in the first unbroken fiber for a 5 fiber composite in which the first two fibers and all matrix layers before the first unbroken fiber are broken calculate three different ways. For the $E_f/E_m = 16.667$ results, $E_f = 40000$ MPa, $G_f = 16667$ MPa, $E_m = 2400$ MPa, $G_f = 902.25$ MPa, and $V_f = 0.5$. For the $E_f/E_m = 1.6667$ results, E_m was increased to 24000 MPa.

and rewriting the boundary condition equations accordingly. Finally, all shape functions (L_i and R_i) were assumed to be linear.

Fiber stresses in unidirectional composites can also be determined using an interlayer shear-lag method. The governing equations are in eq. (71). Such a Hedgepeth-type analysis for a finite number of fibers is available in the literature (Nairn, 1988a; Nairn, 1988b); the analysis from those papers was used here except for a minor difference in the calculation of V_f which leads to a scaling factor that must be changed for comparison to the above optimal shear-lag results. An advantage of the interlayer method for these unidirectional composite problems is that the eigenvalues and eigenvectors of the key matrix (see eq. (74)) can be found analytically (Nairn, 1988a; Nairn, 1988b).

Figure 9 plots the axial stress in the third fiber (layer 6) as a function of distance from the plane of the crack. These calculations were for layers 1 to 5 being broken. The results from both an optimal, shear-lag and an interlayer, shear-lag analysis are compared to finite element calculations (FEA). The two sets of results are for two different ratios between the fiber and matrix moduli. For *high-contrast* composites (or E_f/E_m large), both shear-lag methods agreed well with FEA results. The optimal analysis was always between the interlayer analysis and FEA results and thus was always more accurate than interlayer analysis. The differences were larger for the *low-contrast* composite. When E_f/E_m was low, the optimal analysis still agreed reasonably well with FEA results. The interlayer method, however, got worse. The peak axial stress at $y = 0$ is the stress concentration in the first unbroken fiber. By an interlayer analysis, the stress concentration is independent of E_f/E_m. FEA calculations show that it is not independent of E_f/E_m and the optimal analysis agreed with the FEA results.

To probe stress concentration calculations further, we calculated the stress concentration in the first unbroken fiber as a function of fiber volume fraction. The two calculations in Fig. 10 are for when the matrix layer just before the first unbroken fiber was either broken or intact. A characteristic of an interlayer analysis is that this stress concentration factor is independent of the fiber and matrix properties, independent of the fiber volume fraction, and insensitive to whether or not the last matrix layer is broken. The FEA results (symbols), however, show that the interlayer analysis is wrong; the stress concentration factor does

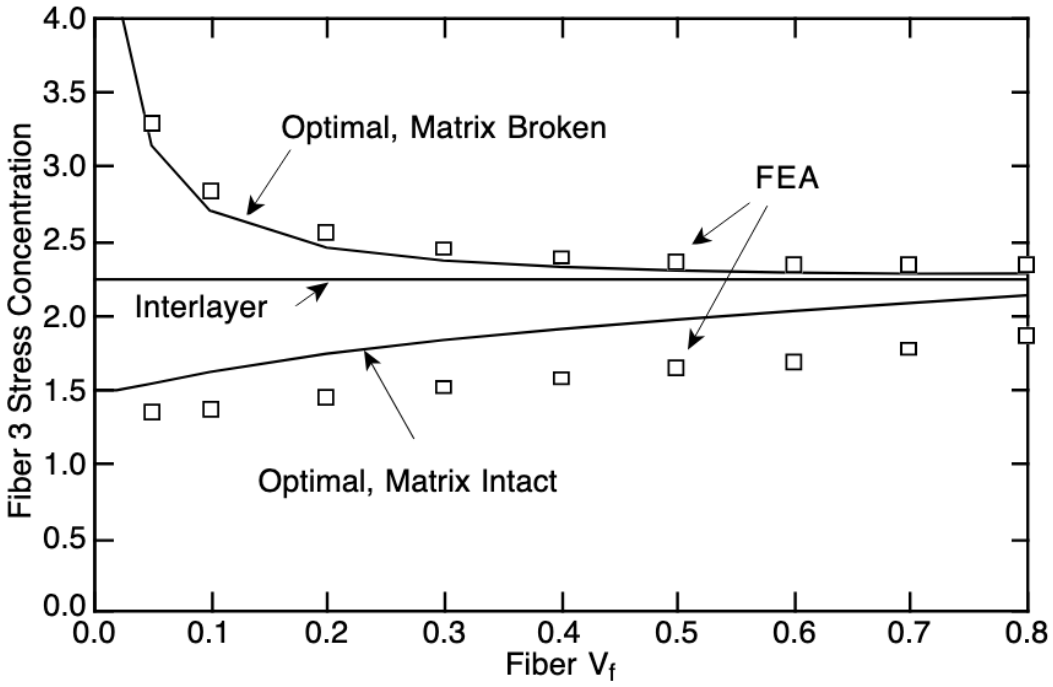

Fig. 10. Stress concentration is the first unbroken fiber (fiber 3 or layer 6) as a function of the fiber volume fraction calculated three ways. The two cases analyzed are when the matrix layer neighboring the first unbroken fiber is either broken or intact. The fiber and matrix properties are given in the caption of Fig. 9 (for $E_f/E_m = 16.667$.

depend on V_f and on the state of the last matrix layer. The optimal shear-lag analysis can calculate these effects. It agreed very well with FEA results when the neighboring matrix layer was broken and reasonably well when that matrix layer was intact. The interlayer, shear-lag method is best described as a limiting analysis that is only correct in the limit as $E_fV_f/E_mV_m \to \infty$. In other words, all results converge to the interlayer result in the limit as $V_f \to 1$. An interlayer analysis is thus not capable of doing calculations about the effect of E_fV_f/E_mV_m. Because the matrix carries no load, interlayer analysis is also incapable of analyzing the effect of cracks in matrix layers. This limitation to *high-contrast* composites is a property of interlayer, shear-lag analysis; it is not an inherent property of shear-lag methods. When shear-lag analysis is done more accurately using an optimal, shear-lag analysis, it can be used for any E_fV_f/E_mV_m ratio and it can investigate matrix cracking effects.

4. Conclusions

By starting from elasticity theory for planar stress analysis problems, it was possible to derive shear-lag equations for analysis of stress-transfer problems in multilayered composite materials. The first shear-lag equations were derived with only three assumptions:

1. The fundamental shear-lag assumption in eq. (3) that defines a "shear-lag" analysis.
2. An assumed form for the shear stresses in each layer (see eq. (20)).
3. An assumption that simplifies Hooke's law for each layer (see eq. (30)).

We termed this analysis the *Optimal, Shear-Lag Analysis* because it used the fewest assumptions possible for derivation of shear-lag equations. The sample calculations in the **Examples** section show that optimal, shear-lag analysis can accurately calculate axial stresses, shear stresses, and total energy in many composite stress analysis problems. The key equation to solve is given in eq. (45). The solution can be derived by

an eigen-analysis. Improved accuracy can sometimes be obtained by adjusting of the shear-stress shape functions for each particular problem.

Very few shear-lag analyses of composites use the optimal, shear-lag analysis derived here. Most previous shear-lag methods use sub-optimal methods that require additional assumptions not required in the optimal, shear-lag analysis. For example, by additionally assuming that all stiff layers are interspersed with compliant interlayers and that the axial displacements are linear in each layer, it was possible to derive shear-lag equations that are commonly used for stress analysis of composites. We termed these two approaches *Interlayer, Shear-Lag Analysis* and *Parametric, Interlayer, Shear-Lag Analysis*. The first interlayer method means problems where the interlayers correspond to actual physical layers; the second means problems where the interlayers correspond to *fictitious* layers with *effective* shear properties. These interlayer methods are always less accurate than optimal, shear-lag analysis. These sub-optimal methods have sometimes given shear-lag analysis a reputation for being fairly crude. In many problems, the methods in this paper can be used to easily replace sub-optimal methods by optimal methods and thereby to convert crude models into more accurate models. Sometimes this change can be done with no additional mathematical complexity; sometimes optimal methods require more involved calculations.

There is a common misconception that shear-lag methods can only be used for composite structures in which the modulus ratios between the layers is very high. That belief is true for interlayer methods. This modulus ratio effect, however, is not inherent to shear-lag methods. None of the above three assumptions used for the optimal, shear-lag analysis require any assumption about the moduli of the layers. The results in the **Examples** section show that optimal, shear-lag analysis works well for layers with any relative moduli. An interlayer, shear-lag analysis might be an acceptable method for a polymer adhesive with metal adherends or for polymer-matrix composite problems with stiff fibers. It should never be used, however, for problems with phases having closer moduli, such as for ceramic- or metal-matrix composites. For such problems, an optimal, shear-lag analysis might offer an useful replacement.

Acknowledgment — This work was supported by a grant from the Mechanics of Materials program at the National Science Foundation (CMS-9713356). David-A. Mendels was supported by the Swiss National Science Fundation.

5. Appendix

Because of the simple form of $\boldsymbol{\tau}_0$, the i^{th} element of $\boldsymbol{\tau}_\infty = [B]^{-1}\boldsymbol{\tau}_0$ can be written as

$$(\boldsymbol{\tau}_\infty)_i = \frac{B^{-1}_{i,1}}{E^{(1)}_y t_1}\tau_0 + \frac{B^{-1}_{i,n-1}}{E^{(n)}_y t_n}\tau_n \tag{109}$$

The elements of the inverse of the $[B]$ matrix can be written as

$$B^{-1}_{i,j} = \frac{\text{cof}_{j,i}([B])}{\det[B]} \tag{110}$$

where $\text{cof}_{j,i}([B])$ if the (j,i) cofactor of matrix $[B]$ and $\det[B]$ is the determinant of matrix $[B]$. Because of the tridiagonal form of $[B]$, it can be proved by induction that

$$\det[B] = \frac{tE^0_y}{\prod_{i=1}^{n} E^{(i)}_y t_i} \tag{111}$$

This result can be then be used to show that

$$\text{cof}_{1,i}([B]) = \frac{\sum_{j=i+1}^{n} E^{(j)}_y t_j}{\prod_{j=2}^{n} E^{(j)}_y t_j} \qquad \text{and} \qquad \text{cof}_{n-1,i}([B]) = \frac{\sum_{j=1}^{i} E^{(j)}_y t_j}{\prod_{j=1}^{n-1} E^{(j)}_y t_j} \tag{112}$$

Substitution of these results into eq. (109) leads to the result in eq. (38).

6. REFERENCES

Bailey, J. E., P. T. Curtis and A. Parvizi, 1979. On the Transverse Cracking and Longitudinal Splitting Behavior of Glass and Carbon Fibre Epoxy Cross-Ply Laminates and the Effect of Poisson and Thermally Generated Strains, *Proc. R. Soc. Lond. A 366*, 599.

Caslini, M., C. Zanotti, and T. K. O'Brien, 1987. Fracture Mechanics of Matrix Cracking and Delamination in Glass/Epoxy Laminates, *J. Comp. Tech & Research Winter*, 121.

Cox, H. L., 1952. The Elasticity and Strength of Paper and Other Fibrous Materials, *Brit. J. Appl. Phys. 3*, 72.

Dharani, L. R., W. F. Jones, and J. G. Goree, 1983. Mathematical Modeling of Damage in Unidirectional Composites, *Eng. Fract. Mech. 17*, 555.

Dharani, L. R. and H. Tang, 1990. Micromechanics Characterization of Sublaminates Damage, *Int'l J. Fracture 46*, 123.

Eringren, A. C. and B. S. Kim, 1974. Stress Concentration in Filamentary Composites with Broken Fibers, *Letters in Applied and Engineering Sciences 2*, 69.

Flaggs, D. L., 1985. Prediction of Tensile Matrix Failure in Composite Laminates, *J. Comp. Mat. 19*, 29.

Garrett, K. W. and J. E. Bailey, 1977. Multiple Transverse Fracture in 90° Cross-Ply Laminates of a Glass Fibre-Reinforced Polyester, *J. Mat. Sci 12*, 157.

Gau, Y. C., Y. M. Mai, and B. Cotterell, 1988. Fracture of Fiber-Reinforced Materials, *J. Appl. Math. and Phys. 39*, 550.

Goree, J. G. and R. S. Gross, 1979a. Stresses in a Three-Dimensional Unidirectional Composite Containing Broken Fibers, *Eng. Fract. Mech. 13*, 395.

Goree, J. G. and R. S. Gross, 1979b. Analysis of a Unidirectional Composite Containing Broken Fibers and Matrix Damage, *Eng. Fract. Mech. 13*, 563.

Han, Y. M., H. T. Hahn, and R. B. Croman, 1987. A Simplified Analysis of Transverse Ply Cracking in Cross-Ply Laminates. *Proc. Amer. Soc. of Comp.,* 2^{nd} *Tech. Conf.*, Newark, DE, September 23-25.

Han, Y. M., H. T. Hahn, and R. B. Croman, 1987. A Simplified Analysis of Transverse Ply Cracking in Cross-Ply Laminates, *Comp. Sci. & Tech. 31*, 165.

Hedgepeth, J. M., 1961. Stress Concentrations in Filamentary Structures. *NASA TN D-882*.

Hedgepeth, J. M. and P. Van Dyke, 1967. Local Stress Concentrations in Imperfect Filamentary Composite Materials, *J. Comp. Mat. 1*, 294.

Hsueh, C. H., 1988. Elastic Load Transfer From Partially Embedded Axially Loaded Fibre to Matrix, *J. Mat. Sci. Letts 7*, 497.

Hsueh, C. H., 1995. Modeling of Elastic Stress Transfer in Fiber-Reinforced Composites, *Trends in Polymer Science 10*, 336.

Kim, J. K., C. Baillie, and Y. M. Mai, 1991. Interfacial Debonding and Fibre Pull-Out Stresses. Part I: Critical Comparison of Existing Theories, *J. Mat. Sci. 27*, 3143.

Kulkarni, S. V., B. W. Rosen, and C. Zweben, 1973. Load Concentration Factors for Circular Holes in Composite Laminates, *J. Comp. Mat. 7*, 387.

Lacroix, Th., B. Tilmans, R. Keunings, M. Desaeger, and I. Verpoest, 1992. Modeling of Critical Fibre Length and Interfacial Debonding in the Fragmentation Testing of Polymer Composites, *Comp. Sci. & Tech. 43*, 379.

Laws, N. and G. J. Dvorak, 1988. Progressive Transverse Cracking in Composite Laminates, *J. Comp. Mat. 22*, 900.

Lekhnitski, S. G., 1981. *Theory of an Anisotropic Body*, MIR Publishers, Moscow.

Liu, C. H. and J. A. Nairn, 1999. Analytical Fracture Mechanics of the Microbond Test Including the Effects of Friction and Thermal Stresses, *J. of Adhes. and Adhesives. 19*, 59.

Manders, P. W., T. W. Chou, F. R. Jones, and J. W. Rock, 1983. Statistical Analysis of Multiple Fracture in [0/90/0] Glass fiber/epoxy resin laminates, *J. Mat. Sci. 19*, 2876.

McCartney, L. N., 1992. Analytical Models of Stress Transfer in Unidirectional Composites and Cross-Ply Laminates, and Their Application to the Prediction of Matrix/Transverse Cracking, *Local Mechanics Concepts for Composite Material Systems*, eds., J. N. Reddy and K. L Reifsnider, Proc. IUTAM Symposium, Blacksburg, VA, 251.

McCartney, L. N., 1996. Stress Transfer Mechanics for Ply Cracks in General Symmetric Laminates. *NPL Report CMMT(A)50*.

McCartney, L. N. and C. Pierce, 1997. Stress Transfer Mechanics for Multiple Ply Laminates for Axial Loading and Bending. *Proc. ICCM-11*, Gold Coast, Australia.

McManus, H. L. and J. R. Maddocks, 1996. On Microcracking in Composite Laminates Under Thermal and Mechanical Loading, *Polymers & Polymer Composites 4*, 305.

Mendels, D.-A., S. A. Page, Y. Leterrier, J.-A. E. Månson, and J. A. Nairn, 2000. A Modified Double lap-Shear Test As A Mean To Measure Intrinsic Properties of Adhesive Joints. *Proc. of ECCM 9*, Brighton, UK, June 4-7.

Nairn, J. A., 1988a. Fracture Mechanics of Unidirectional Composites Using the Shear-Lag Model I: Theory, *J. Comp. Mat. 22*, 561.

Nairn, J. A., 1988b. Fracture Mechanics of Unidirectional Composites Using the Shear-Lag Model II: Experiment, *J. Comp. Mat. 22*, 589.

Nairn, J. A., S. Liu, H. Chen, and A. R. Wedgewood, 1990. Longitudinal Splitting in Epoxy and K-Polymer Composites: Shear-Lag Analysis Including the Effect of Fiber Bridging, *J. Comp. Mat. 25*, 1086.

Nairn, J. A., S. Hu, and J. S. Bark, 1993. A Critical Evaluation of Theories for Predicting Microcracking in Composite Laminates, *J. Mat. Sci. 28*, 5099.

Nairn, J. A. and S. Hu, 1994. Micromechanics of Damage: A Case Study of Matrix Microcracking, *Damage Mechanics of Composite Materials*, ed., Ramesh Talreja, Elsevier, Amsterdam, 187.

Nairn, J. A. and H. D. Wagner, 1996. A Revised Shear-Lag Analysis of an Energy Model for Fiber-Matrix Debonding, *Adv. Comp. Letts. 5*, 131.

Nairn, J. A., 1997. On the Use of Shear-Lag Methods for Analysis of Stress Transfer in Unidirectional Composites, *Mech. of Materials 26*, 63.

Nairn, J. A., 2000. Matrix Microcracking in Composites, *Polymer Matrix Composites*, R. Talreja and J.-A. E. Månson, eds., Vol. 2 of *Comprehensive Composite Materials*, A. Kelly and C. Zweben,. eds., Elsevier Science, 403.

Nayfeh, A. H., 1977. Thermomechanically Induced Interfacial Stresses in Fibrous Composites, *Fibre Sci. & Tech. 10*, 195.

Phoenix, S. L. and I. J. Beyerlein, 2000. Statistical Strength Theory for Fibrous Composite Materials, *Fiber Reinforcements and General Theory of Composites*, T. W. Chou, ed., Vol. 1 of *Comprehensive Composite Materials*, A. Kelly and C. Zweben,. eds., Elsevier Science, 559.

Piggott, M. R., 1987. Debonding and Friction at Fiber-Polymer Interfaces. I: Criteria for Failure and Sliding, *Comp. Sci. & Tech. 30*, 295.

Press, W. H., B. P. Flannery, S. A. Teukolsky, and W. T. Vetterling, 1988. *Numerical Recipes in C*, Cambridge University Press, New York.

Reifsnider, K. L., 1977. Some Fundamental Aspects of the Fatigue and Fracture Response of Composite Materials. *Proc.* 14^{th} *Annual Meeting of SES, Lehigh, PA, November*, Lehigh, PA, November.

Tan, S. C. and R. J. Nuismer, 1989. A Theory for Progressive Matrix Cracking in Composite Laminates, *J. Comp. Mat. 23*, 1029.

Timoshenko, S. P.and J. N. Goodier, 1970. *Theory of Elasticity, Third Edition*, McGraw-Hill Book Company, New York.

Zhou, L. M., J. K. Kim, and Y. M. Mai, 1992. Interfacial Debonding and Fiber Pull-Out Stresses. Part II: A New Model Based on the Fracture Mechanics Approach, *J. Mat. Sci. 27*, 3155.